Journal of South American Earth Sciences 47 (2013) 100–115

Contents lists available at ScienceDirect

Journal of South American Earth Sciences

journal homepage: www.elsevier.com/locate/jsames

U–Pb ages and metamorphic evolution of the La Pampa Gneisses: Implications for the evolution of the Chilenia Terrane and Permo-Triassic tectonics of north Central Chile

Javier Álvarez [a,*], Constantino Mpodozis [b], Idael Blanco-Quintero [c,d], Antonio García-Casco [d,e], César Arriagada [a], Diego Morata [a]

[a] Departamento de Geología, Universidad de Chile, Plaza Ercilla 803, Santiago, Chile
[b] Antofagasta Minerals, Apoquindo 4001, Piso 18, Santiago, Chile
[c] Departamento de Geociencias, Universidad de Los Andes, Bogotá, Colombia
[d] Departamento de Mineralogía y Petrología, Universidad de Granada, Spain
[e] Instituto Andaluz de Ciencias de la Tierra, Spain

ARTICLE INFO

Article history:
Received 11 February 2013
Accepted 11 July 2013

Keywords:
Chilenia
Zircon
P-T-t path
Metamorphism
Paleozoic
North-central Chile

ABSTRACT

The La Pampa Gneisses are an enclave of orthogneisses emplaced within late Paleozoic to Triassic granitoids of the Chollay Batholith, in the Cordillera Frontal, to the east of Vallenar. Previous geochronological data (a Rb/Sr "errorchron" of 415 ± 4 Ma) allowed to some authors to suggest that these rocks were part of the Chilenia Terrane accreted to Gondwana during the Middle Devonian (*ca.* 390 Ma). New petrographic, chemical and geothermobarometric studies, together with U–Pb geochronological data show that the protolith of the La Pampa Gneisses derives from peraluminous tonalites emplaced during the Pennsylvanian at 306.5 ± 1.8 Ma, ruling out the hypothesis considering these rocks as remnant of the pre-collisional Chilenia basement. The tonalites were metamorphosed between 5.06 and 5.58 kbar and 709–779 °C during the middle Permian (267.6 ± 2.1 Ma), possibly in conjunction with the San Rafael tectonic event and the emplacement of the oldest granitoids of the Chollay Batholith. A new intrusive episode occurred at *ca.* 240 Ma, followed by exhumation and cooling during a regional Triassic extensional episode.

1. Introduction: the Chilenia problem

During most of the Paleozoic, Gondwana and Laurentia were separated by the Iapetus Ocean, and the western margin of Gondwana records a complex history of subduction, collision of microplates and accretion of terranes (Ramos, 2009; Ramos et al., 1984, 1986; Astini et al., 1995; Rapela et al., 1998; Thomas and Astini, 2003a, b; Cawood, 2005). A variety of allocthonous and/or para-autocthonous terranes (Pampia, Famatina, Arequipa-Antofalla and Cuyania) were amalgamated to the stable Río de la Plata and Amazonia cratons during the early Paleozoic (Fig. 1). In central Argentina and Chile, the latest terrane which would become part of Gondwana is the hypothetical Chilenia Terrane (Ramos et al., 1984, 1986), probably accreted to South America during the Middle Devonian (Davis et al., 1999, 2000; Ramos, 2009; Willner et al., 2008, 2011). However, unlike other terranes such as Pampia or Cuyania (Rapela et al., 1998; Ramos, 2009, 2010), rock outcrops that can be attributed to Chilenia are unknown and no direct evidences for its original affiliation are available.

Various authors have proposed that the eastern limit of Chilenia is represented by a string of ultramafic bodies and metamorphic lenses located between the Cordillera Frontal and the Western Precordillera over at least 300 km length from 30° to 34° S. One of these, the Guarguaraz Complex, composed of serpentinite lenses, metabasites and garnet-bearing metasedimentary rocks exposed at the Cordón del Portillo in the Cordillera Frontal, southwest of Mendoza (Fig. 1; Ramos and Basei, 1997; Keppie and Ramos, 1999; López de Azarevich et al., 2009; González-Menéndez et al., 2013), has been interpreted as part of a continental margin later deeply buried within the collision zone between Chilenia and the previously accreted Cuyania Terrane (Massonne and Calderón, 2008; Davis et al., 1999, 2000). Davis et al. (1999) obtained an Ar/Ar age of 384.5 ± 0.5 Ma in neocrystallized white mica from a phyllite sample of the Guarguaraz Complex, which was interpreted as the

* Corresponding author.
E-mail address: javalvar@cec.uchile.cl (J. Álvarez).

0895-9811/$ – see front matter © 2013 Elsevier Ltd. All rights reserved.
http://dx.doi.org/10.1016/j.jsames.2013.07.001

age of the deformation and metamorphism caused by the collision. More recently, Willner et al. (2011) reported three four-point Lu/Hf mineral isochrons from metapelite and metabasite, which yield an average age of 390.0 ± 2.2 Ma, which they also interpreted as the time of the collision between Chilenia and Cuyania. To the west, Chilenia seems to be bounded by accretionary complexes developed along the subduction system built along its trailing edge after its collision with Gondwana, and now preserved along the Chilean Coastal Cordillera, including the Huasco (Moscoso et al., 1982; Godoy and Wellkner, 2003; Welkner et al., 2006), Choapa (Irwin et al., 1988; Willner et al., 2008) and the Central Chile metamorphic complexes (Hervé, 1988; Hervé et al., 2012, Fig. 1).

The Chilenia basement appears, however, to be largely covered by late Paleozoic to Cenozoic sedimentary and volcanic rocks and intruded by late Paleozoic to Triassic batholiths. A supporting argument for the continental nature of Chilenia can be found in the geochemical signatures of the late Paleozoic to Triassic igneous rocks of the Cordillera Frontal (Kay et al., 1989; Mpodozis and Kay, 1990, 1992; Llambías, 1999) whose geochemistry indicates an important contribution of melts derived from a continental crust (Mpodozis and Kay, 1990, 1992). Recently, Álvarez et al. (2011) argued in favor of the existence of Chilenia based on the age of a population of detrital zircon grains in the El Tránsito Metamorphic Complex. This unit has an important group of zircon grains of *ca*. 570–535 Ma, an age that is absent in known igneous or metamorphic rocks from Chile and Argentina, suggesting a source likely located in the Chilenia Terrane. The same age group of detrital zircons has been also identified within the Choapa and Huasco metamorphic complexes (Willner et al., 2008; Álvarez et al., 2011) and in the Guarguaraz and Filo Gris complexes (Astini and Cawood, 2009).

One of the few rock units that have been attributed to Chilenia are the Las Yaretas Gneisses, that crops out at the Cordón del Portillo, Mendoza (Ramos and Basei, 1997; Keppie and Ramos, 1999). However, López de Azarevich et al. (2009) considerer this unit as slices of the eastern Grenvillian-age Cuyania basement, which were tectonically incorporated into the Guarguaraz Complex during the collision with Chilenia. More recently, Astini and Cawood (2009) suggested the Filo Gris Complex, located in the Cordillera Frontal of La Rioja, Argentina, and formed by mottled phyllites and metagreywakes (including a 570–535 Ma population of detrital zircons), as part of a sedimentary blanket deposited on top of the Chilenia Terrane before its final accretion to Gondwana.

One of the few places where Paleozoic metamorphic units occur in the Chilean Frontal Cordillera is the El Tránsito valley region, to the east of the city of Vallenar (29°S; Fig. 1), where Ribba et al. (1988) recognized a, two km in diameter, sub circular enclave of migmatitic gneisses within the Elqui–Limarí Batholith, and termed them the La Pampa Gneisses (Figs. 1 and 2). These are the only outcrop of rocks which potentially belongs to the Chilenia basement recognized so far in Chile. A Rb/Sr "errorchron" of 415 ± 4 Ma was the main argument in favor to the assignment of this unit to Chilenia (Ribba et al., 1988).

In this contribution we present a combined geochronological (zircon U–Pb ages), geochemical and geothermobarometric study of the La Pampa Gneisses. These new data together with new zircon U–Pb ages from the enclosing intrusive rocks will allow us to determine the age, origin, and the possible links to Chilenia and to the Late Paleozoic geodynamic evolution of the Pacific margin of Central Chile and Argentina.

2. Basement geology of the El Tránsito valley region

Fig. 2 is a simplified geological map of part of the El Tránsito river valley, showing the distribution of metamorphic and plutonic

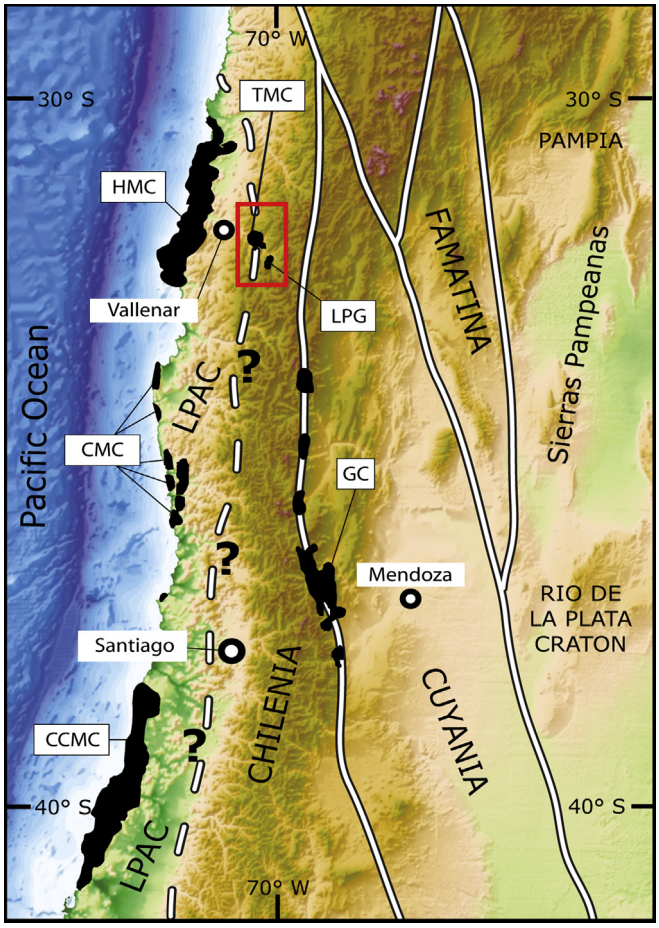

Fig. 1. Map of tectonostratigraphic terranes of central Chile and Argentina, showing the approximate position of terrane sutures (thick white lines). In black, outcrops of the main metamorphic complexes and units discussed in the text. LPAC: Late Paleozoic Accretionary Complexes; TMC: El Tránsito Metamorphic Complex; HMC: Huasco Metamorphic Complex; LPG: La Pampa Gneisses; CMC: Choapa Metamorphic Complex; GC: Guarguaraz Complex; CCMC: Central Chile Metamorphic Complex. Red rectangle shows the study area and corresponds to the geological map of Fig. 2. Terrane boundaries modified from Ramos (2009). (For interpretation of the references to colour in this figure legend, the reader is referred to the web version of this article.)

rocks of the Cordillera Frontal basement. The area can be divided in two tectonic domains separated by the Pinte Fault, a major N–S trending basin-controlling normal fault that represents an extensional regime during the Mesozoic and was reactivated as reverse during later stages of the Andean orogeny (Reutter, 1974; Ribba et al., 1988; Salazar et al., 2012).

2.1. The Eastern domain

Along the southeast corner of the study area, the eastern domain includes the outcrops of the La Pampa Gneisses which are intruded by granitoid plutons of the Chollay Batholith and surrounded by a migmatitic aureole (Fig. 2). A N–S elongated belt of mylonitic rocks (El Portillo Mylonites) derived from an igneous protolith (Ribba, 1985; Murillo, 2012) appears to the west of the La Pampa Gneisses, and, as the Chollay Batholith plutons, are unconformably covered by Triassic lavas and Jurassic marine sedimentary rocks (Reutter, 1974; Ribba et al., 1988; Salazar et al., 2012, Fig. 2).

Ribba et al. (1988) described the La Pampa Gneisses as banded orthogneisses with potassium feldspar, plagioclase, quartz, biotite

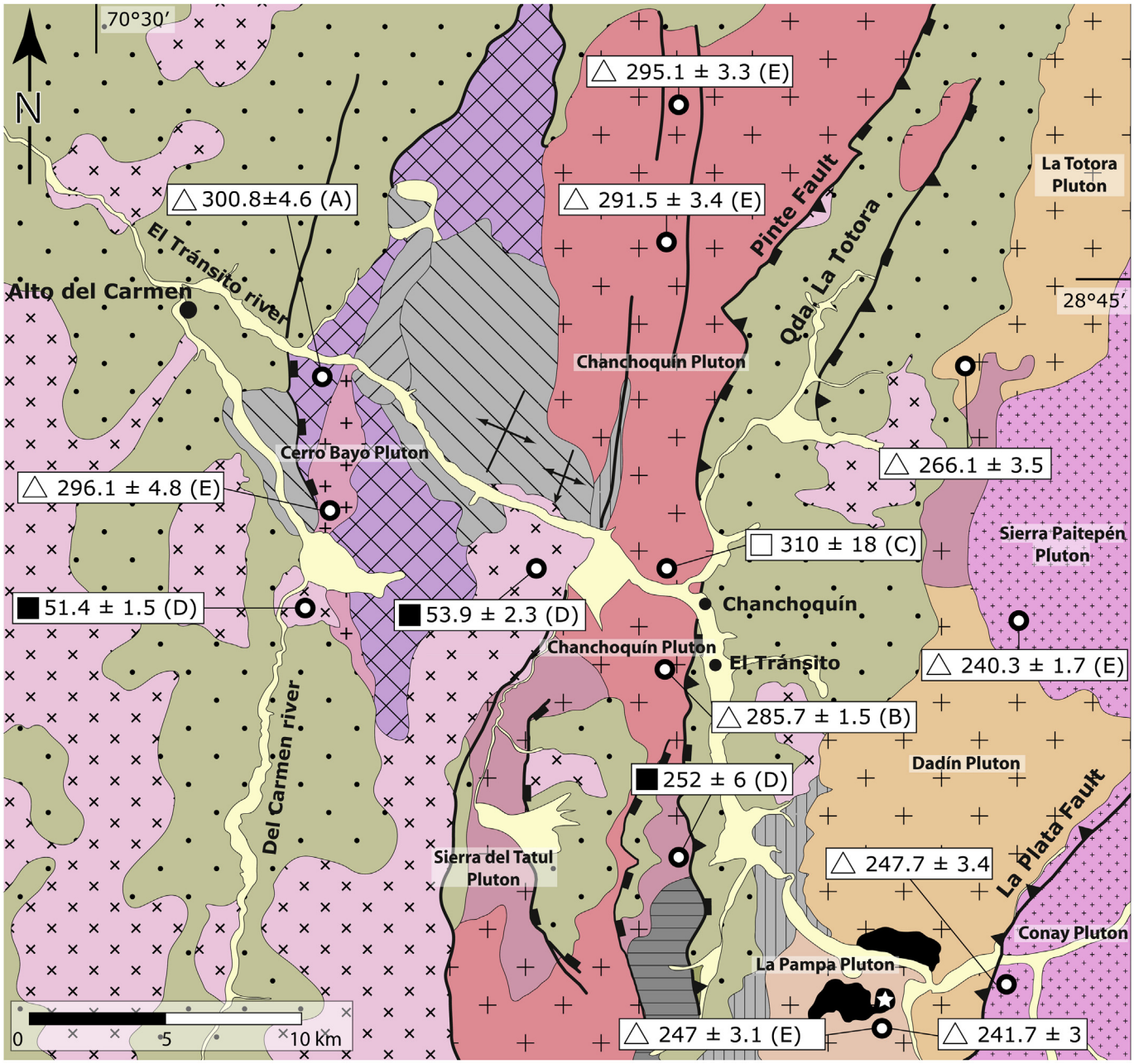

Fig. 2. Simplified geological map of the El Tránsito valley area, east of Vallenar.

Table 1
Zircon U–Pb geochronological analytical data.

Sample	Concentration		Isotope ratios				Apparent ages (Ma)				Best age	Error	Disc
	U (ppm)	Th/U	^{238}U / ^{206}Pb	Error (%)	^{207}Pb / ^{206}Pb	Error (%)	^{206}Pb 238U	Error 1-s	^{207}Pb / ^{206}Pb	Error 1-s	(Ma)	1-s	(%)
JA01-1	517.2	0.09	23.82	2.12	0.0582	1.12	265.1	5.5	536.2	24.3	265.1	5.5	51
JA01-2	1388.4	0.15	41.68	2.43	0.0557	0.78	152.8	3.7	440.2	17.3	152.8	3.7	65
JA01-3	326.0	0.27	23.51	1.56	0.0525	0.93	268.5	4.1	305.8	20.9	268.5	4.1	12
JA01-4	388.1	0.24	23.77	1.51	0.0519	0.88	265.7	3.9	280.8	20.1	265.7	3.9	5
JA01-5	241.9	0.20	24.54	1.53	0.0543	0.96	257.4	3.9	381.7	21.4	257.4	3.9	33
JA01-6	332.4	0.24	23.87	1.46	0.0520	0.89	264.6	3.8	286.8	20.3	264.6	3.8	8
JA01-7	210.1	0.18	22.81	1.86	0.0515	1.12	276.6	5.0	261.1	25.6	276.6	5.0	−6
JA01-8	398.8	0.15	26.00	1.86	0.0661	1.88	243.3	4.4	809.7	38.8	243.3	4.4	70
JA01-9	241.0	0.24	23.40	1.58	0.0616	1.20	269.7	4.2	661.7	25.6	269.7	4.2	59
JA01-10	778.7	0.16	27.80	1.55	0.0596	0.83	227.8	3.5	590.4	18.0	227.8	3.5	61
JA01-11	286.7	0.17	23.64	1.68	0.0552	0.90	267.1	4.4	422.0	20.0	267.1	4.4	37
JA01-12	353.2	0.19	24.32	1.82	0.0534	0.90	259.8	4.6	344.3	20.3	259.8	4.6	25
JA01-13	509.3	0.28	24.11	1.65	0.0514	0.87	261.9	4.2	259.7	19.8	261.9	4.2	−1
JA01-14	176.5	0.28	23.80	1.64	0.0526	1.00	265.4	4.3	312.2	22.5	265.4	4.3	15
JA01-15	97.9	0.19	24.40	1.80	0.0514	1.28	258.9	4.6	260.7	29.2	258.9	4.6	1
JA01-16	611.6	0.13	24.27	2.03	0.0528	1.02	260.3	5.2	321.5	23.1	260.3	5.2	19
JA01-17	474.1	0.17	24.01	2.01	0.0563	1.10	263.1	5.2	464.9	24.3	263.1	5.2	43
JA01-18	201.6	0.06	25.31	2.09	0.0537	1.16	249.8	5.1	358.8	25.9	249.8	5.1	30
JA01-19	379.9	0.17	22.51	1.99	0.0531	1.07	280.2	5.4	332.0	24.0	280.2	5.4	16
JA01-21	81.5	0.30	21.29	2.04	0.0892	1.41	295.9	5.9	1407.7	26.8	295.9	5.9	79
JA01-22	377.4	0.18	24.02	1.91	0.0513	1.07	262.9	4.9	254.9	24.3	262.9	4.9	−3
JA01-23	270.8	0.20	23.47	1.86	0.0584	1.10	269.0	4.9	543.5	23.8	269.0	4.9	51
JA01-24	586.0	0.50	27.20	2.11	0.0591	1.03	232.7	4.8	572.5	22.2	232.7	4.8	59
JA01-25	564.9	0.36	25.09	1.92	0.0538	1.02	252.0	4.7	362.4	22.9	252.0	4.7	30
JA01-26	164.2	0.21	24.22	1.91	0.0512	1.18	260.9	4.9	248.4	27.0	260.9	4.9	−5
JA01-27	599.1	0.14	22.75	1.92	0.0661	1.08	277.3	5.2	808.9	22.5	277.3	5.2	66
JA01-28	168.2	0.24	23.61	2.01	0.0615	1.76	267.5	5.3	657.5	37.4	267.5	5.3	59
JA01-29	257.2	0.53	24.57	3.10	0.0618	1.53	257.1	7.8	665.6	32.3	257.1	7.8	61
JA01-30	777.1	0.48	24.19	1.85	0.0518	0.97	261.1	4.7	274.6	22.0	261.1	4.7	5
JA01-31	210.3	0.19	23.11	2.60	0.0921	1.25	273.1	7.0	1469.8	23.5	273.1	7.0	81
JA01-32	467.7	0.20	22.70	2.27	0.0522	1.10	277.9	6.2	295.2	25.0	277.9	6.2	6
JA01-33	324.3	0.16	23.49	2.33	0.0525	1.16	268.8	6.1	308.1	26.3	268.8	6.1	13
JA01-34	306.0	0.14	18.31	3.06	0.0580	1.20	342.8	10.2	529.3	26.0	342.8	10.2	35
JA01-35	275.1	0.24	24.63	2.42	0.0524	1.15	256.5	6.1	303.1	26.1	256.5	6.1	15
JA01-36	242.1	0.19	23.78	2.36	0.0521	1.16	265.5	6.1	288.2	26.4	265.5	6.1	8
JA01-38	135.6	0.37	23.70	2.24	0.0521	1.28	266.4	5.9	288.3	29.1	266.4	5.9	8
JA01-39	282.9	0.23	23.60	2.11	0.0523	1.15	267.6	5.5	298.7	26.1	267.6	5.5	10
JA01-40	603.9	0.57	23.07	2.26	0.0584	1.07	273.5	6.0	543.5	23.3	273.5	6.0	50
JA01-41	343.6	0.53	23.32	3.51	0.0580	1.32	270.6	9.3	528.7	28.7	270.6	9.3	49
JA01-42	285.1	0.25	22.43	2.16	0.0560	1.17	281.1	5.9	452.7	25.7	281.1	5.9	38
JA01-44	2158.3	0.75	41.78	2.67	0.1153	1.23	152.5	4.0	1884.4	22.1	152.5	4.0	92
JA01-45	304.4	0.75	22.53	2.23	0.0762	1.21	279.9	6.1	1100.0	24.1	279.9	6.1	75
JA01-46	320.2	0.28	23.06	1.60	0.0599	0.97	273.6	4.3	598.9	24.4	273.6	4.3	54
JA01-47	423.6	0.18	23.90	1.71	0.0528	0.98	264.2	4.4	318.8	25.8	264.2	4.4	17
JA01-48	266.8	0.24	23.56	1.60	0.0526	1.03	268.0	4.2	310.4	26.8	268.0	4.2	14
JA01-49	601.9	0.01	24.34	1.51	0.0527	0.92	259.6	3.9	317.5	24.8	259.6	3.9	18
JA01-50	413.6	0.14	21.62	1.66	0.0529	0.93	291.5	4.7	324.3	24.8	291.5	4.7	10
JA01-51	46.2	0.16	23.85	2.02	0.0525	1.85	264.8	5.2	308.8	43.6	264.8	5.2	14
JA01-52	278.5	0.25	23.34	1.59	0.0529	1.01	270.5	4.2	322.5	26.4	270.5	4.2	16
JA01-53	619.1	0.10	24.26	1.59	0.0534	0.92	260.4	4.1	346.2	24.6	260.4	4.1	25
JA01-54	699.0	0.07	23.24	1.66	0.0579	0.94	271.6	4.4	526.9	24.2	271.6	4.4	48
JA01-55	153.2	0.28	23.65	1.50	0.0521	1.12	267.0	3.9	290.9	28.7	267.0	3.9	8
JA02-1	1016.6	0.32	26.68	1.43	0.0519	0.87	237.2	3.3	280.8	23.9	237.2	3.3	16
JA02-2	193.8	0.65	25.68	1.79	0.0517	1.08	246.2	4.3	271.9	27.9	246.2	4.3	9
JA02-3	74.4	0.38	26.11	1.82	0.0541	1.52	242.3	4.3	373.9	36.2	242.3	4.3	35
JA02-4	82.1	0.42	25.49	1.67	0.0529	1.46	248.0	4.1	325.0	35.4	248.0	4.1	24
JA02-5	282.6	0.34	25.29	1.63	0.0533	1.04	250.0	4.0	340.8	26.9	250.0	4.0	27
JA02-6	276.7	0.27	23.35	2.28	0.0547	1.14	270.4	6.0	398.9	28.6	270.4	6.0	32
JA02-7	892.1	0.41	25.30	2.08	0.0634	0.98	249.8	5.1	722.4	24.2	249.8	5.1	65
JA02-12	1188.8	0.29	25.50	1.65	0.0537	1.00	248.0	4.0	358.9	22.5	248.0	4.0	31
JA02-13	235.7	0.58	24.09	1.69	0.0588	1.26	262.2	4.3	559.3	27.2	262.2	4.3	53
JA02-14	157.5	0.63	25.25	1.60	0.0534	1.23	250.4	3.9	344.3	27.6	250.4	3.9	27
JA02-15	183.9	0.33	25.41	1.58	0.0521	1.17	248.8	3.9	288.5	26.6	248.8	3.9	14
JA02-16	1184.5	0.26	25.91	1.42	0.0622	1.07	244.1	3.4	680.5	22.8	244.1	3.4	64
JA02-17	161.9	0.35	25.65	1.54	0.0545	1.21	246.5	3.7	391.7	27.0	246.5	3.7	37
JA02-18	608.0	0.38	24.05	1.49	0.0521	1.01	262.6	3.8	290.7	23.0	262.6	3.8	10
JA02-20	1367.3	0.26	26.36	1.94	0.0522	1.19	240.0	4.6	293.0	26.8	240.0	4.6	18
JA02-21	54.3	0.36	25.12	1.93	0.0509	1.67	251.6	4.8	237.2	38.1	251.6	4.8	−6
JA02-22	112.2	0.55	24.94	1.70	0.0512	1.32	253.5	4.2	251.2	30.1	253.5	4.2	−1
JA02-23	191.4	0.42	26.18	1.61	0.0529	1.18	241.6	3.8	325.0	26.6	241.6	3.8	26

(*continued on next page*)

Table 1 (*continued*)

Sample	Concentration		Isotope ratios				Apparent ages (Ma)				Best age	Error	Disc
	U (ppm)	Th/U	^{238}U / ^{206}Pb	Error (%)	^{207}Pb / ^{206}Pb	Error (%)	^{206}Pb / 238U	Error 1-s	^{207}Pb / ^{206}Pb	Error 1-s	(Ma)	1-s	(%)
JA02-24	113.9	0.43	25.56	1.70	0.0509	1.33	247.4	4.1	238.4	30.4	247.4	4.1	−4
JA02-25	455.1	0.32	25.43	1.55	0.0512	1.07	248.6	3.8	251.9	24.3	248.6	3.8	1
JA02-26	1319.0	0.32	25.34	2.04	0.0979	1.42	249.5	5.0	1583.8	26.4	249.5	5.0	84
JA02-27	671.5	0.32	25.12	2.03	0.0535	0.98	251.6	5.0	349.3	22.0	251.6	5.0	28
JA02-28	373.7	0.20	26.43	2.08	0.0563	1.13	239.4	4.9	464.6	24.8	239.4	4.9	48
JA02-29	466.7	0.26	24.98	2.13	0.0521	0.99	253.0	5.3	290.6	22.6	253.0	5.3	13
JA02-30	219.3	0.30	24.41	2.17	0.0541	1.13	258.8	5.5	375.0	25.1	258.8	5.5	31
JA02-31	669.6	0.19	25.54	2.25	0.0544	1.01	247.6	5.5	389.5	22.5	247.6	5.5	36
JA02-32	1004.6	0.31	28.13	2.51	0.0964	1.81	225.2	5.6	1556.4	33.6	225.2	5.6	86
JA02-33	137.0	0.41	25.39	2.19	0.0513	1.22	249.0	5.3	255.1	27.9	249.0	5.3	2
JA02-34	149.0	0.38	27.22	2.25	0.0519	1.30	232.6	5.1	282.1	29.5	232.6	5.1	18
JA02-35	168.1	0.32	24.38	2.51	0.0568	1.37	259.2	6.4	484.6	30.0	259.2	6.4	47
JA02-36	100.1	0.39	23.30	2.54	0.0564	1.42	270.8	6.7	466.3	31.2	270.8	6.7	42
JA02-37	108.1	0.32	23.41	2.58	0.0558	1.46	269.6	6.8	443.0	32.2	269.6	6.8	39
JA02-38	1137.1	0.15	26.01	2.46	0.0528	1.06	243.2	5.9	322.2	24.0	243.2	5.9	25
JA02-39	447.2	0.30	25.02	2.41	0.0528	1.19	252.6	6.0	319.9	26.8	252.6	6.0	21
JA02-40	160.8	0.66	26.03	2.58	0.0593	1.54	243.0	6.2	578.3	33.2	243.0	6.2	58
JA02-41	299.3	0.36	24.86	2.47	0.0654	1.56	254.2	6.1	788.2	32.4	254.2	6.1	68
JA02-42	159.8	0.40	26.63	2.48	0.0512	1.38	237.7	5.8	248.4	31.5	237.7	5.8	4
JA02-44	1024.6	0.18	24.15	2.42	0.1015	1.78	261.5	6.2	1652.6	32.7	261.5	6.2	84
JA02-45	60.2	0.43	25.57	3.05	0.0554	1.92	247.3	7.4	429.3	42.2	247.3	7.4	42
JA02-46	1306.2	0.27	26.23	3.08	0.0546	1.23	241.2	7.3	395.8	27.3	241.2	7.3	39
JA02-47	87.3	0.30	25.80	2.78	0.0547	2.11	245.1	6.7	398.4	46.6	245.1	6.7	38
JA02-48	238.6	0.80	25.23	2.47	0.0515	1.22	250.6	6.1	263.0	27.7	250.6	6.1	5
JA02-49	90.9	0.46	25.07	2.42	0.0527	1.56	252.2	6.0	317.9	35.0	252.2	6.0	21
JA02-50	197.5	0.60	26.90	2.40	0.0514	1.34	235.3	5.5	260.3	30.4	235.3	5.5	10
JA05-0	118.9	0.29	20.87	1.97	0.0534	1.25	301.7	5.8	347.9	28.0	301.7	5.8	13
JA05-1	291.9	0.56	20.75	2.17	0.0502	1.43	303.4	6.4	202.3	32.8	303.4	6.4	−50
JA05-2	92.2	0.46	23.97	12.67	0.0520	3.13	263.5	32.6	284.5	70.0	263.5	32.6	7
JA05-3	470.8	0.26	12.79	2.07	0.0575	1.16	485.2	9.7	511.9	25.3	485.2	9.7	5
JA05-4	648.6	0.48	15.24	2.18	0.0561	1.09	409.7	8.6	456.3	24.0	409.7	8.6	10
JA05-5	195.4	0.31	6.96	1.97	0.0678	1.16	865.3	15.9	862.8	23.9	865.3	15.9	0
JA05-6	675.0	0.55	19.35	1.99	0.0525	1.12	324.7	6.3	305.9	25.4	324.7	6.3	−6
JA05-7	610.2	0.46	19.84	2.16	0.0521	1.28	317.0	6.7	291.6	29.0	317.0	6.7	−9
JA05-8	1544.1	0.29	20.27	3.22	0.0535	1.08	310.5	9.7	348.9	24.2	310.5	9.7	11
JA05-9	1231.0	0.15	26.08	1.99	0.0515	1.08	242.6	4.7	264.6	24.5	242.6	4.7	8
JA05-10	382.9	0.85	14.38	2.02	0.0564	1.15	433.5	8.5	468.3	25.2	433.5	8.5	7
JA05-11	545.4	0.97	22.48	2.06	0.0557	1.17	280.6	5.6	438.5	25.8	280.6	5.6	36
JA05-12	68.2	2.00	5.96	2.27	0.0724	1.42	999.5	21.0	998.6	28.6	999.5	21.0	0
JA05-13	126.0	0.65	23.45	5.59	0.0805	4.87	269.2	14.7	1208.2	93.0	269.2	14.7	78
JA05-14	223.8	1.20	13.91	2.16	0.0559	1.21	447.7	9.3	448.7	26.7	447.7	9.3	0
JA05-15	413.7	0.45	24.20	2.17	0.0511	1.55	261.1	5.5	246.8	35.3	261.1	5.5	−6
JA05-16	369.0	0.64	13.28	2.12	0.0548	1.33	468.0	9.5	403.7	29.5	468.0	9.5	−16
JA05-17	1002.0	0.47	24.54	1.86	0.0516	1.16	257.5	4.7	268.8	26.5	257.5	4.7	4
JA05-18	562.0	0.33	19.43	1.90	0.0519	1.26	323.5	6.0	282.4	28.5	323.5	6.0	−15
JA05-19	216.3	0.35	4.73	2.00	0.0858	1.16	1235.4	22.4	1333.9	22.3	1333.9	22.3	7
JA05-20	592.9	0.37	9.71	1.95	0.0605	1.12	632.0	11.7	620.7	24.0	632.0	11.7	−2
JA05-21	404.5	0.72	21.21	1.97	0.0523	1.33	297.0	5.7	298.6	30.0	297.0	5.7	1
JA05-23	192.0	0.25	11.76	1.97	0.0578	1.34	526.1	10.0	524.1	29.1	526.1	10.0	0
JA05-24	1799.3	0.12	5.25	1.79	0.0788	1.03	1123.3	18.5	1166.0	20.2	1166.0	20.2	4
JA05-25	222.6	0.19	28.30	3.08	0.0506	1.84	223.9	6.8	222.6	41.9	223.9	6.8	−1
JA05-26	478.7	0.96	12.14	1.90	0.0575	1.17	510.2	9.3	510.5	25.6	510.2	9.3	0
JA05-27	149.4	0.42	6.11	2.72	0.0718	1.34	976.5	24.6	980.5	27.0	976.5	24.6	0
JA05-28	263.7	0.51	11.77	2.06	0.0580	1.28	525.8	10.4	529.6	27.8	525.8	10.4	1
JA05-29	41.9	0.63	23.93	2.69	0.0514	2.82	263.9	6.9	259.6	63.5	263.9	6.9	−2
JA05-30	341.2	0.12	12.93	2.02	0.0557	1.28	480.3	9.3	439.0	28.3	480.3	9.3	−9
JA05-31	678.8	0.33	5.40	1.97	0.0763	0.84	1094.7	19.8	1102.8	16.8	1102.8	16.8	1
JA05-32	1155.4	0.52	14.22	2.03	0.0547	0.90	438.0	8.6	399.6	20.1	438.0	8.6	−10
JA05-33	642.2	0.67	23.95	2.16	0.0583	1.20	263.7	5.6	541.4	26.0	263.7	5.6	51
JA05-34	272.5	0.20	5.41	2.18	0.0747	0.96	1093.1	21.9	1061.6	19.2	1061.6	19.2	−3
JA05-35	916.9	0.43	19.68	2.11	0.0522	0.99	319.5	6.6	294.5	22.4	319.5	6.6	−8
JA05-36	1358.2	0.29	20.17	2.00	0.0519	0.92	311.9	6.1	281.4	21.0	311.9	6.1	−11
JA05-37	371.2	0.34	22.98	2.22	0.0518	1.19	274.5	6.0	278.1	27.1	274.5	6.0	1
JA05-38	924.5	0.30	5.42	2.03	0.0757	0.86	1092.2	20.3	1087.4	17.1	1087.4	17.1	0
JA05-39	792.8	0.52	22.73	2.11	0.0522	1.06	277.6	5.7	296.2	24.1	277.6	5.7	6
JA05-40	119.4	0.34	23.83	2.27	0.0514	1.83	265.0	5.9	258.9	41.5	265.0	5.9	−2
JA05-41	373.9	0.67	21.45	2.18	0.0529	1.14	293.8	6.2	323.0	25.7	293.8	6.2	9
JA05-42	191.1	0.62	21.01	3.18	0.0571	1.78	299.8	9.3	495.4	38.8	299.8	9.3	39
JA05-43	670.1	0.36	20.94	2.40	0.0517	1.12	300.7	7.1	272.0	25.5	300.7	7.1	−11
JA05-44	551.1	0.57	21.79	2.18	0.0509	1.16	289.3	6.2	236.3	26.6	289.3	6.2	−22
JA05-45	301.9	0.63	20.97	2.08	0.0524	1.27	300.2	6.1	303.6	28.7	300.2	6.1	1
JA94-93	990.1	0.54	26.10	0.01	0.0526	0.01	242.3	3.1	310.3	22.6	242.3	3.1	22

Table 1 (*continued*)

Sample	Concentration		Isotope ratios				Apparent ages (Ma)				Best age	Error	Disc
	U (ppm)	Th/U	^{238}U / ^{206}Pb	Error (%)	^{207}Pb / ^{206}Pb	Error (%)	^{206}Pb / 238U	Error 1-s	^{207}Pb / ^{206}Pb	Error 1-s	(Ma)	1-s	(%)
JA94-90	606.5	0.77	26.10	0.01	0.0524	0.01	242.3	3.3	300.8	24.8	242.3	3.3	19
JA94-89	460.8	0.56	25.94	0.01	0.0564	0.01	243.9	3.2	467.8	24.8	243.9	3.2	48
JA94-88	289.1	0.54	26.48	0.01	0.0528	0.01	239.0	3.2	322.1	31.0	239.0	3.2	26
JA94-87	329.3	0.68	26.30	0.02	0.0563	0.02	240.5	3.6	462.8	33.8	240.5	3.6	48
JA94-83	218.6	1.13	26.07	0.02	0.0532	0.01	242.7	3.7	337.6	30.0	242.7	3.7	28
JA94-82	844.1	0.76	26.29	0.02	0.0524	0.02	240.6	3.7	301.4	36.5	240.6	3.7	20
JA94-81	470.9	0.77	26.52	0.01	0.0501	0.01	238.6	3.1	201.1	26.6	238.6	3.1	−19
JA94-77	852.3	0.98	25.77	0.01	0.0512	0.01	245.4	2.6	247.8	27.0	245.4	2.6	1
JA94-76	582.3	0.69	26.10	0.01	0.0507	0.01	242.4	2.6	227.5	28.4	242.4	2.6	−7
JA94-74	623.9	0.90	26.72	0.01	0.0523	0.01	236.9	2.8	297.3	29.3	236.9	2.8	20
JA94-73	625.9	0.81	26.07	0.01	0.0510	0.01	242.7	2.7	239.4	26.8	242.7	2.7	−1
JA94-72	286.9	0.70	26.46	0.01	0.0537	0.01	239.1	2.8	360.1	30.5	239.1	2.8	34
JA94-71	486.5	1.01	26.19	0.01	0.0510	0.01	241.6	2.7	241.4	28.3	241.6	2.7	0
JA94-65	624.0	0.65	25.82	0.01	0.0531	0.01	244.9	2.7	333.2	26.6	244.9	2.7	26
JA94-63	821.7	0.73	26.43	0.01	0.0515	0.01	239.4	2.5	264.4	26.4	239.4	2.5	9
JA94-59	519.6	1.32	26.01	0.01	0.0506	0.01	243.2	2.5	224.3	26.2	243.2	2.5	−8
JA94-56	281.8	1.26	26.34	0.01	0.0504	0.01	240.2	2.9	213.8	31.2	240.2	2.9	−12
JA94-55	356.4	0.70	26.46	0.01	0.0508	0.01	239.1	2.5	233.1	26.3	239.1	2.5	−3
JA94-54	455.8	0.68	26.18	0.01	0.0519	0.01	241.7	2.5	278.9	27.8	241.7	2.5	13
JA94-53	494.3	0.71	26.09	0.01	0.0520	0.01	242.4	2.5	287.0	26.0	242.4	2.5	16
JA94-52	294.3	0.53	26.50	0.01	0.0548	0.01	238.8	2.7	403.2	31.2	238.8	2.7	41
JA94-50	808.8	0.84	25.97	0.01	0.0533	0.01	243.5	2.3	341.8	23.9	243.5	2.3	29
JA94-48	1450.2	1.76	26.14	0.01	0.0513	0.01	242.0	2.4	252.6	22.1	242.0	2.4	4
JA94-47	354.8	1.44	26.55	0.02	0.0562	0.06	238.4	5.0	459.6	120.4	238.4	5.0	48
JA94-46	384.8	0.75	26.27	0.01	0.0508	0.01	240.8	2.6	230.4	29.3	240.8	2.6	−4
JA94-45	733.5	0.93	25.93	0.01	0.0522	0.01	243.9	2.5	293.3	26.9	243.9	2.5	17
JA94-42	336.6	0.98	26.03	0.01	0.0512	0.01	243.0	2.6	250.5	27.4	243.0	2.6	3
JA94-41	467.0	0.61	25.97	0.01	0.0512	0.01	243.6	2.4	251.6	26.0	243.6	2.4	3
JA94-40	728.9	0.85	25.93	0.01	0.0515	0.01	243.9	2.7	261.7	26.3	243.9	2.7	7
JA94-39	282.5	0.89	26.31	0.01	0.0501	0.01	240.5	3.1	199.9	30.8	240.5	3.1	−20
JA94-37	501.8	0.69	26.25	0.01	0.0501	0.01	241.1	2.7	197.4	26.6	241.1	2.7	−22
JA94-34	408.3	1.15	25.91	0.01	0.0513	0.01	244.1	2.9	252.8	27.4	244.1	2.9	3
JA94-30	590.1	1.52	26.38	0.01	0.0515	0.01	239.8	2.7	262.6	26.6	239.8	2.7	9
JA94-27	815.4	0.88	26.22	0.01	0.0515	0.01	241.3	2.7	261.9	25.4	241.3	2.7	8
JA94-25	800.4	0.82	26.15	0.01	0.0508	0.01	241.9	2.6	231.5	24.7	241.9	2.6	−4
JA94-24	400.7	0.76	26.29	0.01	0.0512	0.01	240.7	2.9	249.8	28.6	240.7	2.9	4
JA94-22	589.5	0.75	25.88	0.01	0.0510	0.01	244.4	2.8	239.1	27.0	244.4	2.8	−2
JA94-21	519.8	0.89	26.29	0.01	0.0549	0.01	240.7	3.0	408.7	23.8	240.7	3.0	41
JA94-20	710.7	0.75	26.19	0.01	0.0533	0.01	241.5	3.0	341.5	20.4	241.5	3.0	29
JA94-19	682.3	0.70	25.81	0.01	0.0519	0.01	245.0	3.0	279.8	20.0	245.0	3.0	12
JA94-17	822.1	0.75	26.06	0.01	0.0509	0.01	242.7	3.1	235.5	19.7	242.7	3.1	−3
JA94-12	359.0	0.59	25.62	0.01	0.0520	0.01	246.9	3.6	285.7	33.1	246.9	3.6	14
JA94-5	936.3	1.05	26.06	0.01	0.0535	0.01	242.8	3.0	350.6	19.1	242.8	3.0	31
JA94-4	275.0	0.76	25.96	0.01	0.0517	0.01	243.6	3.5	270.7	28.4	243.6	3.5	10

and muscovite, although we have also found cordierite and sillimanite but not potassium feldspar. Geochronological data reported by Ribba et al. (1988) include a poorly defined Rb/Sr bulk rock "errorchron" of 415 ± 4 Ma (MSWD 5.2), a well constrained bulk rock, muscovite and biotite Rb/Sr isochron of 246 ± 18 Ma and two Triassic K/Ar ages of 239 ± 10 Ma (muscovite) and 236 ± 6 Ma (biotite). The Chollay Batholith includes a diverse group of plutons, including the La Pampa Pluton (biotite-hornblende tonalites and two mica tonalites), which intrudes the gneisses to the south of the El Tránsito valley (Fig. 2) and which was dated by Coloma et al. (2012) at 247 ± 3.1 Ma (U–Pb zircon). To the north of the valley, the La Pampa Gneisses are intruded by the Dadín Pluton, (Fig. 2; coarse-grained and foliated biotite-bearing granodiorites). Further north, Coloma et al. (2012) reported a zircon U–Pb age of 240.3 ± 1.7 Ma in the Sierra Paitepén Pluton. Other, but until now non-dated intrusives include coarse-grained and foliated biotite-bearing granodiorites such as those from the La Totora Pluton (Fig. 2) which outcrops in northern part of the study area and pinkish biotite-bearing monzogranites from the Conay Pluton, located to the east of the La Pampa Gneisses outcrops (Fig. 2).

2.2. The Western domain

Metamorphic rocks, including a group of migmatitic gneisses with quartz, biotite white mica, staurolite, plagioclase and garnet (Quebrada Seca Schists; Ribba et al., 1988, Fig. 2) are also observed in the western domain However, the largest metamorphic unit, is the El Tránsito Metamorphic Complex, composed of greenschist, quartz-mica schist, albite-bearing nodular schist, quartzite and marble (Fig. 2) already described and studied by Ribba (1985), Ribba et al. (1988) and Álvarez et al. (2011). Mineral assemblages of the El Tránsito Metamorphic Complex suggest intermediate P-T metamorphic conditions transitional between greenschist and amphibolite facies formed at moderate pressures of up to 5 Kbar (Ribba et al., 1988). Rb/Sr whole rock errorchrons of 304 ± 40, 303 ± 40 and 335 ± 20 Ma may represent the age of a main Carboniferous metamorphic episode (Ribba et al., 1988). K/Ar muscovite ages of 238 ± 10, 231 ± 6 and 229 ± 6 Ma indicate a Triassic cooling event, also recorded by a 248 ± 46 Ma Rb/Sr whole rock errorchron (Ribba et al., 1988). Single-grain U–Pb ages of detrital zircon indicates a maximum Devonian sedimentation age of *ca*. 380 Ma (Álvarez et al., 2011), which precludes any direct

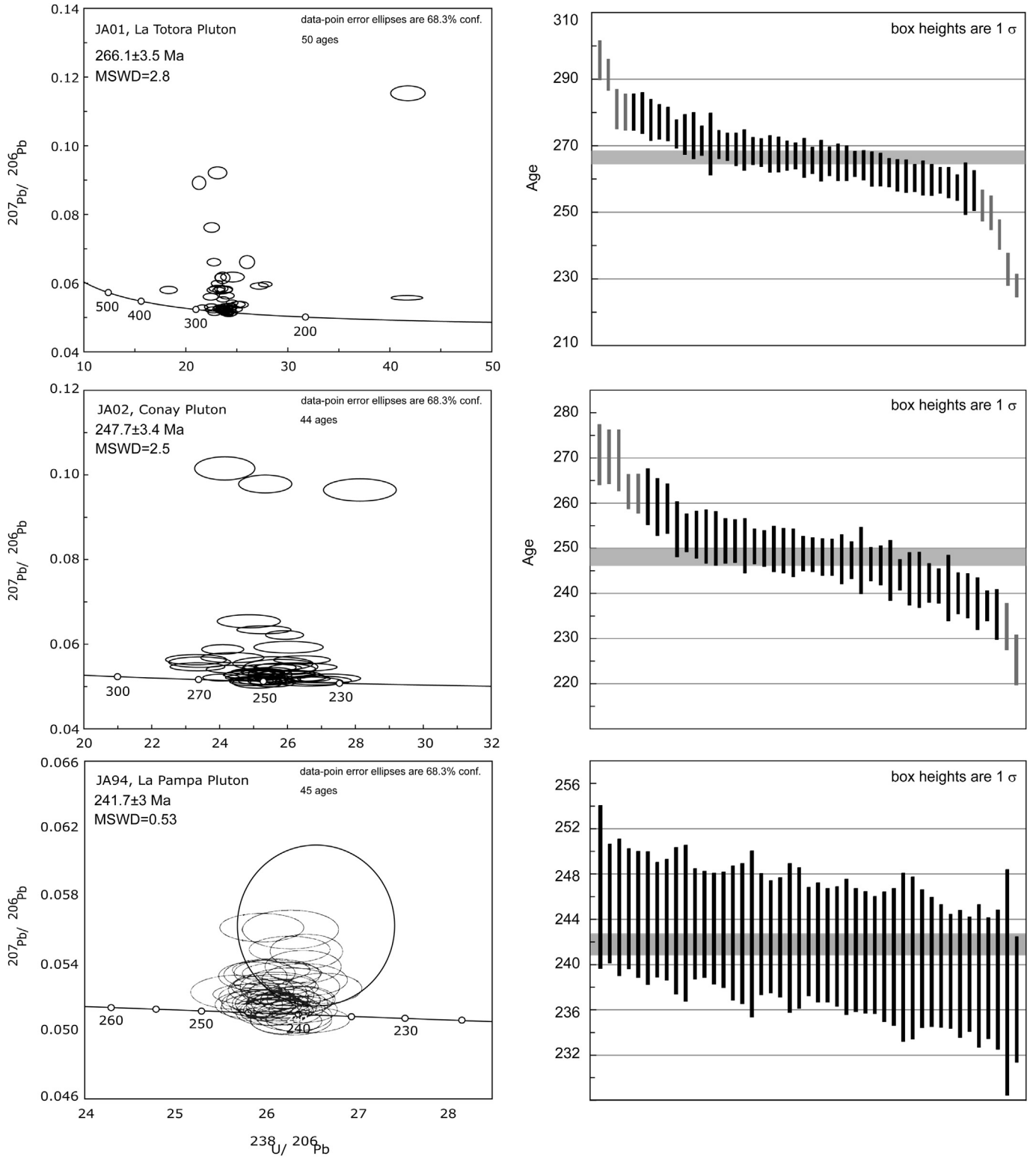

Fig. 3. Tera-Wasserburg plot of U–Pb zircon ages for individual LA-ICP-MS analyses from samples JA01 (La Totora Pluton), JA02 (Conay Pluton), JA94 (La Pampa Pluton), showing the respective weighted average ages.

linkage with the Chilenia pre-collisional basement. The El Tránsito Metamorphic Complex is unconformably covered, to the west, by an acid volcanic and pyroclastic unit (Cerro Bayo Formation; Salazar and Coloma, in prep.) including rhyolitic tuffs dated (U–Pb zircon) at 300.8 ± 4.6 Ma (Salazar et al., 2009) an age which is, slightly older than the 296.1 ± 4.8 Ma U–Pb age reported by Coloma et al. (2012) for a biotite-muscovite-bearing granodiorite from the Cerro Bayo Pluton, that intrudes the volcanic sequence (Fig. 2). Further south, at Río del Carmen, the El Tránsito Metamorphic Complex is covered by Triassic volcanic rocks of the La

Totora Formation and by a thick sequence of marine Triassic conglomerates of the San Félix Formation (Reutter, 1974; Ribba et al., 1988; Mpodozis and Cornejo, 1997, Fig. 2). To the east, the El Tránsito Metamorphic Complex is intruded by Carboniferous to early Permian hornblende-biotite tonalites, granodiorites, and muscovite-biotite granodiorites of the Elqui–Limarí Batholith (Ribba, 1985; Mpodozis and Kay, 1990, 1992) such as the coarse grained biotite-hornblende tonalite of Chanchoquín Pluton which were dated (conventional U–Pb age) at 285.7 ± 1.5 Ma by Pankhurst et al. (1996) although two LA-ICP MS single grain zircon U–Pb ages reported by Coloma et al. (2012) for the northern part of the pluton are somewhat older (295.4 ± 3.3 and 291.5 ± 3.4 Ma, Fig. 2).

3. New geochronological (zircon U–Pb) data for intrusive events in the La Pampa area

In order to obtain a better understanding of the geological framework of the La Pampa Gneisses we dated three samples collected from the La Totora, La Pampa and Conay plutons. Sample location is shown in Fig. 2, U–Pb analytical data are presented in Table 1, while concordia and weighted average age diagrams are shown in Fig. 3, and details of the analytical methods are presented in Appendix A.

Sample JA01 is from the La Totora Pluton was collected ~15 km of the La Pampa Gneisses outcrops (Fig. 2). This sample, petrographically similar to rocks from the Dadín Pluton, which intruded the La Pampa Gneisses is a foliated granodiorite with holocrystalline and inequigranular texture, composed of subhedral quartz with partial wavy extinction, subhedral plagioclase (~2 mm long), sub- and anhedral potassium feldspar, biotite partially replaced by chlorite, white mica (<0.5 mm long) and zircon and apatite as accessory minerals. Zircon ages of this sample plot on or very close to the concordia line, with a calculated U–Pb age of 266.1 ± 3.5 Ma (Fig. 3).

Sample JA94, from the La Pampa Pluton, that intrude the La Pampa Gneisses is a coarse-grained biotite and hornblende tonalite (Fig. 2). This sample shows concordant results for most of the individual grains and yielded a calculated U–Pb age of 241.7 ± 3 Ma (Fig. 3) which is similar to the Triassic (247 ± 3.1 Ma) zircon U–Pb age already reported by Coloma et al. (2012).

Sample JA02, from the Conay Pluton, is a pinkish syenogranite with holocrystalline, inequigranular and isotropic texture, composed of subhedral quartz (<2 mm long), subhedral potassium feldspar (<0.5 mm long) with perthitic texture, subhedral plagioclase (<0.5 mm long), white mica and biotite, and zircon and apatite as accessory minerals. The zircon U–Pb age of this sample (247.7 ± 3.4 Ma), collected to the east of the La Plata Fault (Fig. 2), is similar to the ages obtained for the La Pampa Pluton but, slightly older than others reported for the Conay Pluton by Martin et al. (1999) which include a biotite K/Ar age of 238 ± 6 Ma and two conventional U–Pb zircon ages of 242.5 ± 1.5 Ma and 242 ± 1.5 Ma.

Taken together with previously reported data these new ages show that two pulses of intrusive activity: middle Permian (*ca.* 266 Ma) and middle Triassic (*ca.* 240 Ma) are recorded in the immediate vicinity of the La Pampa Gneisses outcrops.

4. La Pampa Gneisses: petrography, geochemistry and protolith

The La Pampa Gneisses are white to light grey banded migmatitic gneiss with saccaroidal texture and medium to coarse grainsize. Quartz-feldspathic bands alternate with bands rich in biotite showing granoblastic and lepidoblastic textures, respectively. From a total of 4 studied samples, JA05 was chosen to be analyzed in more detail considering its equilibrium textures and representativeness. The mineral assemblage of sample JA05 includes euhedral to subhedral quartz (0.3–1 mm long) with wavy extinction, euhedral to subhedral plagioclase (0.2–1.2 mm long), subhedral biotite (0.5–1.2 mm), euhedral to subhedral muscovite (0.1–0.8 mm), fibrolitic sillimanite and cordierite (~0.5 mm), in addition to ilmenite, zircon and apatite as accessory minerals (Fig. 4). Sillimanite is strongly deformed, whereas quartz and plagioclase are not, suggesting post-kinematic crystallization from a granitic partial melt for the latter minerals. Muscovite partially replaces biotite and cordierite, and shows no deformation (Fig. 4), indicating retrograde growth. The sample contains recrystallized centimetric porphyroclasts of plagioclase and most of the zircon grains show euhedral faces.

A chemical analysis of major elements (in wt% oxides) is presented in Table 2, which shows that the alkali content ($K_2O + Na_2O$) is equal to 4.48 wt% and the silica content is 71, 02 wt%. The Al_2O_3 content is 15.02 wt%, while the $CaO + Na_2O + K_2O$ is 5.68 wt% (Table 2), so the ratio $Al_2O_3/CaO + Na_2O + K_2O$ is >1.

Considering the petrography and major oxides content we conclude that the protolith of the La Pampa Gneisses derives from intrusive rocks, specifically peraluminous tonalites.

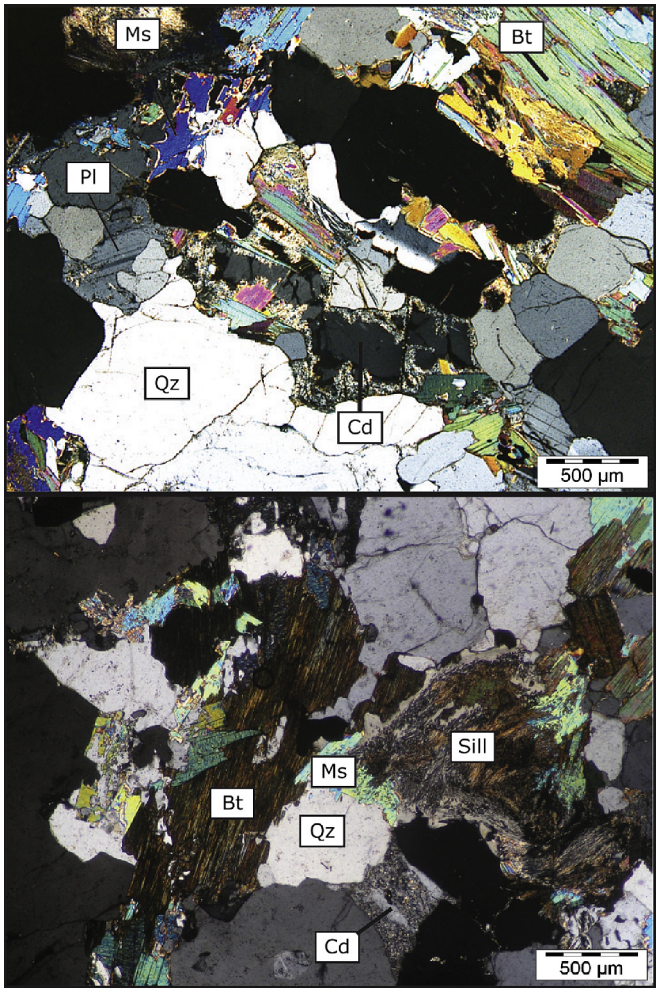

Fig. 4. Microphotographs under plane-polarized light showing textures and mineralogy of the La Pampa Gneisses. Ms: muscovite, Bt: biotite, Pl: plagioclase, Qz: quartz, Cd: cordierite, Sill: sillimanite.

Table 2
Chemical analysis of major elements (in wt% oxides) for the La Pampa Gneisses sample JA05.

Component	%Wt
SiO_2	71.02
TiO_2	0.60
Al_2O_3	15.02
Fe_2O_3	0.86
FeO	3.44
MnO	0.09
MgO	1.45
CaO	1.20
Na_2O	1.75
K_2O	2.73
P_2O_5	0.09
LOI	1.64

5. Zircon U–Pb data from the La Pampa Gneisses

Fig. 5 shows the results of the U–Pb geochronological analysis of La Pampa Gneisses sample JA05 (details in Appendix A). The age of individual zircon grains show a wide range of dispersion from *ca.* 1300 to 260 Ma (Fig. 5). Of a total of 45 analyses, 4 have discordant ages, while 41 plot on, or very close to, the Concordia line (Fig. 5). The density plot distribution shows an old group of Mesoproterozoic zircons ($n = 7$, *ca.* 1300–900 Ma) with Th/U ratios <0.5, except one (Table 1). As 50% of the grains show planar zonation, we conclude considering the Hoskin and Schaltegger (2003) criteria, that this group of zircon grains originated in igneous and metamorphic environments and correspond to inherited crystal cores formed during the Grenville-Sunsas orogeny (Chew et al., 2008; Cordani et al., 2010; Ramos, 2010).

Zircons with Cambrian, Ordovician and Silurian ages constitute a minor population (Fig. 5) and plot in 3 different groups with peaks at *ca.* 523 ($n = 3$), *ca.* 480 ($n = 3$) and *ca.* 440 Ma ($n = 4$). These have Th/U ratios from 0.12 to 1.2 (Table 1), 85.7% of the analyzed grains present non-planar zonation, which suggests a mainly metamorphic and secondary igneous origin (Hoskin and Schaltegger, 2003). This group seems to be composed of inherited cores from rocks formed during the evolution of the Pampean and Famatinian orogenies (Coira et al., 1999; Astini and Dávila, 2004; Schwartz et al., 2008; Ramos, 2009).

Pennsylvanian zircons ($n = 15$) with a peak at 306.5 ± 1.8 Ma constitute the largest population (Fig. 5), 69.3% of the analyzed grains show planar zonation. The Th/U ratio, which varies from 0.29 to 0.97, is in general, >0.5 for planar-zoned zircons and <0.5 for non-planar-zoned zircons and following the Hoskin and Schaltegger (2003) criteria, the data suggest, that most of the Pennsylvanian zircons from sample JA05 have an igneous origin, although some crystals of metamorphic origin are also present. Considering that the closure temperature in the zircon U–Pb system is above 900 °C (Lee et al., 1997) we interpret that the age of the zircons from this group is the age of crystallization of the La Pampa Gneisses protolith.

The youngest population of zircons in sample JA05 has a Permian age, this group constitutes the second major population, with a peak at 267.6 ± 2.1 Ma ($n = 8$) (Fig. 5) and the Th/U ratios ranging from 0.34 to 0.97. Ages of the grains from this youngest group were obtained mainly from the external rim of the zircon grain. 75% of which have textures and zonation indicating a metamorphic origin. We conclude that this age peak is the result of a metamorphic event than can be linked to the Guadalupian magmatic activity represented in the area by intrusives like La Totora Pluton (Fig. 3) dated at 266.1 ± 3.5 Ma.

6. Mineral composition and metamorphism of the La Pampa Gneisses

Representative analyses of the mineral composition of the La Pampa Gneisses are presented in Table 3. The ternary AKF diagram (Fig. 6) projected from appropriate phases and exchange vectors was constructed using the software CSpace (Torres-Roldán et al., 2000). Biotite is not zoned, although its compositional variation is relatively large (Fig. 6) reflecting reequilibration during the P-T evolution of the sample. The most important compositional variations affect Al (1.745–1.883 cations per formula unit, p.f.u.), Fe (1.255–1.522 p.f.u.), Mg (0.809 and 1.068 p.f.u.), Ti (0.070–0.207 p.f.u.) and Na (0.027–0.045 p.f.u.; Table 3). The XMg [Mg/(Mg + Fe) ratio] ranges from 0.359 to 0.441. Muscovite has Si content from 3.019 to 3.068 p.f.u. while Na ranges from 0.098 to 0.122 cations p.f.u. (Table 3), this low to moderate paragonite component suggests a relatively high temperature of formation. Cordierite has XMg in the range 0.560–0.593 (Table 3) and the Na content varies from 0.128 to 0.178. Sample JA05 from the La Pampa Gneisses contains plagioclase and no potassium feldspar. Plagioclase presents normal zonation and has andesine to oligoclase composition, with the albite content ranging from 61 to 76 mol % (Table 3).

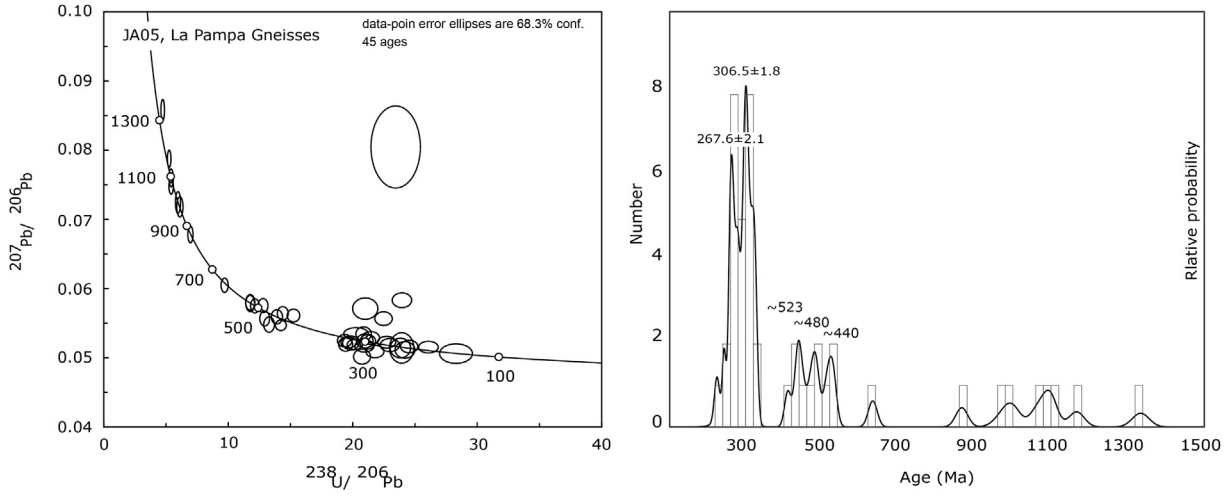

Fig. 5. Tera-Wasserburg plot of U–Pb zircon ages for individual LA-ICP-MS analyses and probability density plot from La Pampa Gneisses sample JA05.

Table 3
Representative mineral analyses of the La Pampa Gneisses sample JA05.

Analisys	Phase	SiO_2	TiO_2	Al_2O_3	Cr_2O_3	FeO	MnO	MgO	CaO	BaO	Na_2O	K_2O	Total	Si	Ti	Al	Cr	Fe	Mn	Mg	Ca	Ba	Na	K	#Mg	Xan	Xab	Xor
JA05-23	bt	34.6	3.4	19.0	0.1	21.6	0.4	6.9	0.0	0.1	0.3	9.2	95.4	2.8	0.2	1.8	0.0	1.4	0.0	0.8	0.0	0.0	0.0	0.9	0.362			
JA05-24	bt	34.7	3.4	19.0	0.0	21.5	0.3	6.8	0.0	0.1	0.3	9.3	95.4	2.8	0.2	1.8	0.0	1.4	0.0	0.8	0.0	0.0	0.0	0.9	0.361			
JA05-25	bt	33.7	2.9	18.5	0.0	22.6	0.4	7.1	0.1	0.1	0.2	8.8	94.3	2.7	0.2	1.8	0.0	1.5	0.0	0.9	0.0	0.0	0.0	0.9	0.359			
JA05-31	bt	33.6	3.4	18.4	0.0	22.2	0.4	7.3	0.0	0.1	0.3	8.8	94.5	2.7	0.2	1.7	0.0	1.5	0.0	0.9	0.0	0.0	0.0	0.9	0.368			
JA05-45	bt	34.5	2.5	19.1	0.0	20.8	0.3	8.2	0.0	0.1	0.2	9.3	95.0	2.7	0.1	1.8	0.0	1.4	0.0	1.0	0.0	0.0	0.0	0.9	0.411			
JA05-46	bt	34.6	2.6	19.3	0.0	21.4	0.3	7.9	0.0	0.0	0.3	9.3	95.7	2.7	0.2	1.8	0.0	1.4	0.0	0.9	0.0	0.0	0.0	0.9	0.397			
JA05-47	bt	34.6	0.5	20.4	0.0	19.2	0.3	9.9	0.0	0.0	0.2	9.2	94.5	2.7	0.0	1.9	0.0	1.3	0.0	1.2	0.0	0.0	0.0	0.9	0.479			
JA05-50	bt	34.2	1.4	19.3	0.0	21.6	0.4	8.7	0.0	0.1	0.2	9.1	95.2	2.7	0.1	1.8	0.0	1.4	0.0	1.0	0.0	0.0	0.0	0.9	0.418			
JA05-51	bt	34.2	1.0	19.7	0.0	20.9	0.3	9.0	0.0	0.0	0.2	9.0	94.4	2.7	0.1	1.8	0.0	1.4	0.0	1.1	0.0	0.0	0.0	0.9	0.433			
JA05-53	bt	34.2	2.1	19.0	0.0	21.6	0.3	8.1	0.0	0.1	0.2	9.3	95.0	2.7	0.1	1.8	0.0	1.4	0.0	1.0	0.0	0.0	0.0	0.9	0.401			
JA05-54	bt	34.6	1.0	19.9	0.0	20.2	0.3	8.9	0.0	0.1	0.2	9.1	94.3	2.7	0.1	1.9	0.0	1.3	0.0	1.0	0.0	0.0	0.0	0.9	0.439			
JA05-73	bt	34.2	2.0	19.1	0.0	21.2	0.3	8.2	0.0	0.1	0.3	9.1	94.6	2.7	0.1	1.8	0.0	1.4	0.0	1.0	0.0	0.0	0.0	0.9	0.408			
JA05-75	bt	34.2	2.0	19.1	0.0	21.3	0.3	8.1	0.0	0.1	0.3	9.1	94.6	2.7	0.1	1.8	0.0	1.4	0.0	1.0	0.0	0.0	0.0	0.9	0.406			
JA05-78	bt	34.4	2.5	19.2	0.0	21.5	0.3	7.8	0.0	0.1	0.3	9.2	95.3	2.7	0.1	1.8	0.0	1.4	0.0	0.9	0.0	0.0	0.0	0.9	0.391			
JA05-83	bt	34.5	2.6	19.2	0.0	21.5	0.3	7.7	0.0	0.1	0.3	9.2	95.3	2.7	0.2	1.8	0.0	1.4	0.0	0.9	0.0	0.0	0.0	0.9	0.389			
JA05-107	bt	34.7	1.2	19.6	0.0	21.0	0.3	8.7	0.0	0.0	0.2	9.4	95.2	2.7	0.1	1.8	0.0	1.4	0.0	1.0	0.0	0.0	0.0	0.9	0.425			
JA05-108	bt	34.6	2.2	19.5	0.0	21.2	0.3	8.0	0.0	0.1	0.3	9.3	95.4	2.7	0.1	1.8	0.0	1.4	0.0	0.9	0.0	0.0	0.0	0.9	0.402			
JA05-109	bt	34.4	1.0	19.6	0.0	20.6	0.4	9.1	0.0	0.1	0.2	9.2	94.6	2.7	0.1	1.8	0.0	1.4	0.0	1.1	0.0	0.0	0.0	0.9	0.441			
JA05-36	chl	24.8	0.1	19.8	0.2	36.1	0.9	4.9	0.1	0.0	0.0	0.4	87.4	5.7	0.0	5.3	0.0	6.9	0.2	1.7	0.0	0.0	0.0	0.1	0.196			
JA05-91	crd	47.8	0.0	32.1	0.0	8.8	0.6	7.2	0.0	0.0	0.6	0.0	97.2	5.0	0.0	3.9	0.0	0.8	0.0	1.1	0.0	0.0	0.1	0.0	0.593			
JA05-92	crd	50.9	0.0	28.2	0.0	9.5	0.5	6.8	0.0	0.0	0.7	0.7	97.4	5.3	0.0	3.5	0.0	0.8	0.0	1.1	0.0	0.0	0.1	0.1	0.560			
JA05-93	crd	47.7	0.0	32.0	0.0	9.2	0.6	6.8	0.0	0.0	0.8	0.0	97.1	5.0	0.0	3.9	0.0	0.8	0.1	1.1	0.0	0.0	0.2	0.0	0.568			
JA05-94	crd	47.8	0.0	32.1	0.0	8.6	0.5	7.0	0.0	0.0	0.9	0.0	97.0	5.0	0.0	3.9	0.0	0.8	0.0	1.1	0.0	0.0	0.2	0.0	0.592			
JA05-95	crd	47.7	0.0	32.2	0.0	9.2	0.6	7.0	0.0	0.0	0.7	0.0	97.5	5.0	0.0	4.0	0.0	0.8	0.0	1.1	0.0	0.0	0.1	0.0	0.577			
JA05-96	crd	47.8	0.0	32.1	0.0	9.0	0.5	6.9	0.0	0.0	0.8	0.0	97.2	5.0	0.0	3.9	0.0	0.8	0.0	1.1	0.0	0.0	0.2	0.0	0.577			
JA05-101	crd	47.9	0.0	32.2	0.0	9.1	0.5	6.8	0.0	0.0	0.7	0.0	97.2	5.0	0.0	4.0	0.0	0.8	0.0	1.1	0.0	0.0	0.2	0.0	0.573			
JA05-104	crd	47.9	0.0	32.3	0.0	8.8	0.5	7.2	0.0	0.0	0.7	0.0	97.5	5.0	0.0	4.0	0.0	0.8	0.0	1.1	0.0	0.0	0.1	0.0	0.593			
JA05-110	crd	47.8	0.0	32.1	0.0	9.6	0.6	6.9	0.0	0.0	0.7	0.0	97.7	5.0	0.0	3.9	0.0	0.8	0.1	1.1	0.0	0.0	0.1	0.0	0.561			
JA05-9	plg	59.1	0.0	25.6	0.0	0.1	0.0	0.0	7.5	0.0	7.8	0.1	100.3	2.6	0.0	1.3	0.0	0.0	0.0	0.0	0.4	0.0	0.7	0.0		0.342	0.650	0.007
JA05-10	plg	62.0	0.0	23.9	0.0	0.2	0.0	0.0	5.2	0.0	9.2	0.1	100.8	2.7	0.0	1.2	0.0	0.0	0.0	0.0	0.2	0.0	0.8	0.0		0.238	0.755	0.008
JA05-11	plg	61.5	0.0	24.0	0.0	0.1	0.0	0.0	5.5	0.0	8.9	0.2	100.2	2.7	0.0	1.2	0.0	0.0	0.0	0.0	0.3	0.0	0.8	0.0		0.250	0.739	0.011
JA05-16	plg	59.7	0.0	25.1	0.0	0.2	0.0	0.0	6.8	0.0	8.1	0.1	100.1	2.6	0.0	1.3	0.0	0.0	0.0	0.0	0.3	0.0	0.7	0.0		0.315	0.678	0.008
JA05-19	plg	60.8	0.0	24.4	0.0	0.3	0.0	0.0	6.0	0.0	8.6	0.2	100.3	2.7	0.0	1.3	0.0	0.0	0.0	0.0	0.3	0.0	0.7	0.0		0.275	0.717	0.008
JA05-32	plg	58.8	0.0	25.8	0.0	0.0	0.0	0.0	7.5	0.0	7.7	0.1	100.0	2.6	0.0	1.4	0.0	0.0	0.0	0.0	0.4	0.0	0.7	0.0		0.348	0.645	0.008
JA05-33	plg	58.2	0.0	26.1	0.0	0.0	0.0	0.0	7.9	0.0	7.4	0.2	99.9	2.6	0.0	1.4	0.0	0.0	0.0	0.0	0.4	0.0	0.6	0.0		0.368	0.621	0.011
JA05-34	plg	62.9	0.0	23.9	0.0	0.0	0.0	0.0	5.0	0.0	9.2	0.2	101.3	2.7	0.0	1.2	0.0	0.0	0.0	0.0	0.2	0.0	0.8	0.0		0.228	0.759	0.013
JA05-35	plg	57.1	0.0	25.0	0.0	0.1	0.0	0.0	7.4	0.0	7.2	0.2	97.0	2.6	0.0	1.4	0.0	0.0	0.0	0.0	0.4	0.0	0.6	0.0		0.360	0.629	0.011
JA05-63	plg	59.9	0.0	25.1	0.0	0.0	0.0	0.0	6.7	0.0	8.3	0.2	100.1	2.7	0.0	1.3	0.0	0.0	0.0	0.0	0.3	0.0	0.7	0.0		0.307	0.685	0.009
JA05-97	plg	58.3	0.0	25.9	0.0	0.0	0.0	0.0	7.7	0.0	7.6	0.2	99.6	2.6	0.0	1.4	0.0	0.0	0.0	0.0	0.4	0.0	0.7	0.0		0.355	0.634	0.010
JA05-99	plg	58.6	0.0	25.8	0.0	0.0	0.0	0.0	7.6	0.0	7.5	0.2	99.8	2.6	0.0	1.4	0.0	0.0	0.0	0.0	0.4	0.0	0.7	0.0		0.356	0.634	0.010
JA05-102	plg	59.2	0.0	25.4	0.0	0.0	0.0	0.0	7.2	0.0	7.8	0.2	99.9	2.6	0.0	1.3	0.0	0.0	0.0	0.0	0.3	0.0	0.7	0.0		0.335	0.654	0.011
JA05-103	plg	58.0	0.0	26.3	0.0	0.0	0.0	0.0	8.2	0.0	7.3	0.2	100.0	2.6	0.0	1.4	0.0	0.0	0.0	0.0	0.4	0.0	0.6	0.0		0.378	0.611	0.011
JA05-105	plg	59.1	0.0	25.5	0.0	0.0	0.0	0.0	7.3	0.0	7.8	0.2	99.9	2.6	0.0	1.3	0.0	0.0	0.0	0.0	0.3	0.0	0.7	0.0		0.337	0.652	0.011
JA05-20	wm	45.0	0.9	34.5	0.1	2.0	0.0	0.5	0.0	0.2	0.7	10.4	94.4	3.0	0.0	2.7	0.0	0.1	0.0	0.1	0.0	0.0	0.1	0.9				
JA05-21	wm	45.2	1.1	34.6	0.0	1.9	0.0	0.5	0.0	0.2	0.8	10.3	94.6	3.0	0.1	2.7	0.0	0.1	0.0	0.0	0.0	0.0	0.1	0.9				

(*continued on next page*)

Table 3 (*continued*)

Analisys	Phase	SiO_2	TiO_2	Al_2O_3	Cr_2O_3	FeO	MnO	MgO	CaO	BaO	Na_2O	K_2O	Total	Si	Ti	Al	Cr	Fe	Mn	Mg	Ca	Ba	Na	K	#Mg	Xan	Xab	Xor
JA05-22	wm	45.1	0.9	34.6	0.0	1.6	0.0	0.5	0.0	0.2	0.8	10.4	94.2	3.0	0.0	2.8	0.0	0.1	0.0	0.0	0.0	0.0	0.1	0.9				
JA05-30	wm	45.0	0.8	35.4	0.0	1.6	0.0	0.4	0.0	0.3	0.8	10.4	94.8	3.0	0.0	2.8	0.0	0.1	0.0	0.0	0.0	0.0	0.1	0.9				
JA05-41	wm	45.3	0.2	35.0	0.0	1.9	0.0	0.6	0.0	0.2	0.8	9.9	93.9	3.1	0.0	2.8	0.0	0.1	0.0	0.1	0.0	0.0	0.1	0.9				
JA05-56	wm	44.8	0.3	35.1	0.0	2.0	0.0	0.5	0.0	0.2	0.8	10.4	94.3	3.0	0.0	2.8	0.0	0.1	0.0	0.1	0.0	0.0	0.1	0.9				
JA05-57	wm	45.1	0.2	34.7	0.0	2.1	0.0	0.6	0.0	0.2	0.8	10.4	94.1	3.0	0.0	2.8	0.0	0.1	0.0	0.1	0.0	0.0	0.1	0.9				
JA05-59	wm	45.1	0.2	35.3	0.0	1.6	0.0	0.5	0.0	0.2	0.9	10.2	94.0	3.0	0.0	2.8	0.0	0.1	0.0	0.1	0.0	0.0	0.1	0.9				
JA05-66	wm	45.0	0.2	35.3	0.1	1.8	0.0	0.5	0.0	0.2	0.8	10.4	94.3	3.0	0.0	2.8	0.0	0.1	0.0	0.1	0.0	0.0	0.1	0.9				
JA05-71	wm	45.2	0.4	36.2	0.0	1.3	0.0	0.5	0.0	0.3	0.9	9.8	94.6	3.0	0.0	2.9	0.0	0.1	0.0	0.0	0.0	0.0	0.1	0.8				
JA05-72	wm	45.1	0.5	34.8	0.0	1.8	0.0	0.6	0.0	0.3	0.8	10.3	94.2	3.0	0.0	2.8	0.0	0.1	0.0	0.1	0.0	0.0	0.1	0.9				
JA05-74	wm	45.1	0.2	35.2	0.0	2.0	0.0	0.6	0.0	0.2	0.8	10.4	94.5	3.0	0.0	2.8	0.0	0.1	0.0	0.1	0.0	0.0	0.1	0.9				
JA05-77	wm	45.4	0.2	35.2	0.1	1.8	0.0	0.6	0.0	0.2	0.8	10.5	94.8	3.0	0.0	2.8	0.0	0.1	0.0	0.1	0.0	0.0	0.1	0.9				
JA05-84	wm	45.3	0.2	35.3	0.0	2.0	0.0	0.6	0.1	0.2	0.8	10.2	94.7	3.0	0.0	2.8	0.0	0.1	0.0	0.1	0.0	0.0	0.1	0.9				
JA05-86	wm	44.9	0.5	35.0	0.0	1.8	0.0	0.5	0.0	0.2	0.8	10.4	94.2	3.0	0.0	2.8	0.0	0.1	0.0	0.1	0.0	0.0	0.1	0.9				
JA05-88	wm	45.4	0.2	34.8	0.0	1.8	0.0	0.6	0.0	0.2	0.8	10.2	94.0	3.1	0.0	2.8	0.0	0.1	0.0	0.1	0.0	0.0	0.1	0.9				
JA05-90	wm	44.3	0.2	34.7	0.0	1.8	0.0	0.6	0.0	0.1	0.8	10.3	92.9	3.0	0.0	2.8	0.0	0.1	0.0	0.1	0.0	0.0	0.1	0.9				
JA05-106	wm	44.9	0.2	35.2	0.0	1.8	0.0	0.5	0.0	0.2	0.8	10.6	94.1	3.0	0.0	2.8	0.0	0.1	0.0	0.0	0.0	0.0	0.1	0.9				

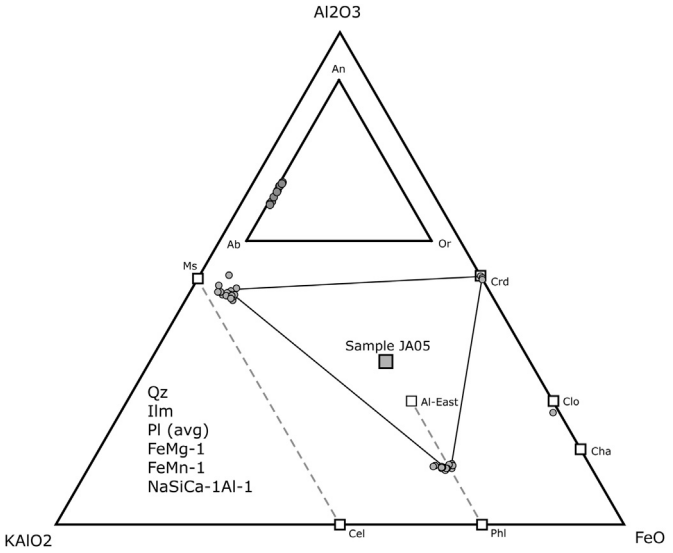

Fig. 6. AKF diagram showing metamorphic assemblage, mineral (grey circles) and whole rock (grey square) chemical composition. Inner triangle represents chemical composition of feldspar analysis. End-members are An: anortite, Ab: albite, Or: orthoclase, Ms: muscovite, Cel: celadonite, Crd: cordierite, Clo: clinochlore, Cha: chamosite, Al-East: aluminum eastonite, Phl: phlogopite. Proyection points are: quartz, ilmenite and average plagioclase; exchange vectors are: FeMg-1, FeMn-1 and NaSiCa-1Al-1.

In order to determine the PT conditions of the La Pampa Gneisses sample JA05, we calculated an isochemical PT projection (i.e., pseudosection) using the bulk chemical analysis of the sample, presented in Table 2 and obtained by ICP-OES (details in Appendix A). The results were constrained with mineral composition analyses obtained by electron microprobe (details in Appendix A).

The calculations were performed for the K_2O–Na_2O–CaO–FeO–MgO–Al_2O_3–SiO_2–Ti_2O–H_2O system using the Perple_X software (Connolly, 2005; version 6.6.7) with the internally consistent thermodynamic data set of Holland and Powell (1998, 2002 upgrade, details in hp02ver.dat file from Perple_X suite). The solution models used are Bio(TCC) (biotite), Gt(HP) (garnet), feldspar (plagioclase and potassic feldspar), IlGkPy (ilmenite-geikielite-pyrophanite solution), hCrd (cordierite), Pheng(HP) (white mica), Chl(HP) (chlorite) and melt(HP) (melt) (details in solution_model.dat file). The fluid in the system was treated as pure H2O using the equation of state of Holland and Powell (1998). Because it is not possible to determine the amount of water during the metamorphism, we treated four isochemical P-T projections with a different water content: 1.64 wt% (LOI), 3 wt%, 4 wt% and, finally, under water saturated conditions. The 1.64 wt%, 3 wt% and water saturated models predict peak metamorphic conditions higher than those calculated for the model with 4 wt% of water (even reaching 800 °C and 6 kbar), this model is more realistic than the previous ones considering the observed peak paragenesis assemblage. Furthermore, the model with saturated conditions was rejected because it predicts that melt appears above 950 °C. The calculation results, pseudosection and calculated isopleths of #Mg in biotite and #Mg in cordierite used to determinate peak P-T conditions, are shown in Fig. 7. Due to the absence of inclusions in the porphyroblasts, pre-peak conditions cannot be estimated. The observed peak metamorphic assemblage of sillimanite, biotite, plagioclase, cordierite and quartz (Fig. 4) corresponds to the field bt-melt-crd-pl-gt-sill-q-ilm (Fig. 7). The presence of melt in this prediction, and the fact that sillimanite is strongly deformed, whereas quartz and plagioclase are not (Fig. 4), suggests that partial melting occurred during prograde metamorphism. Most of the

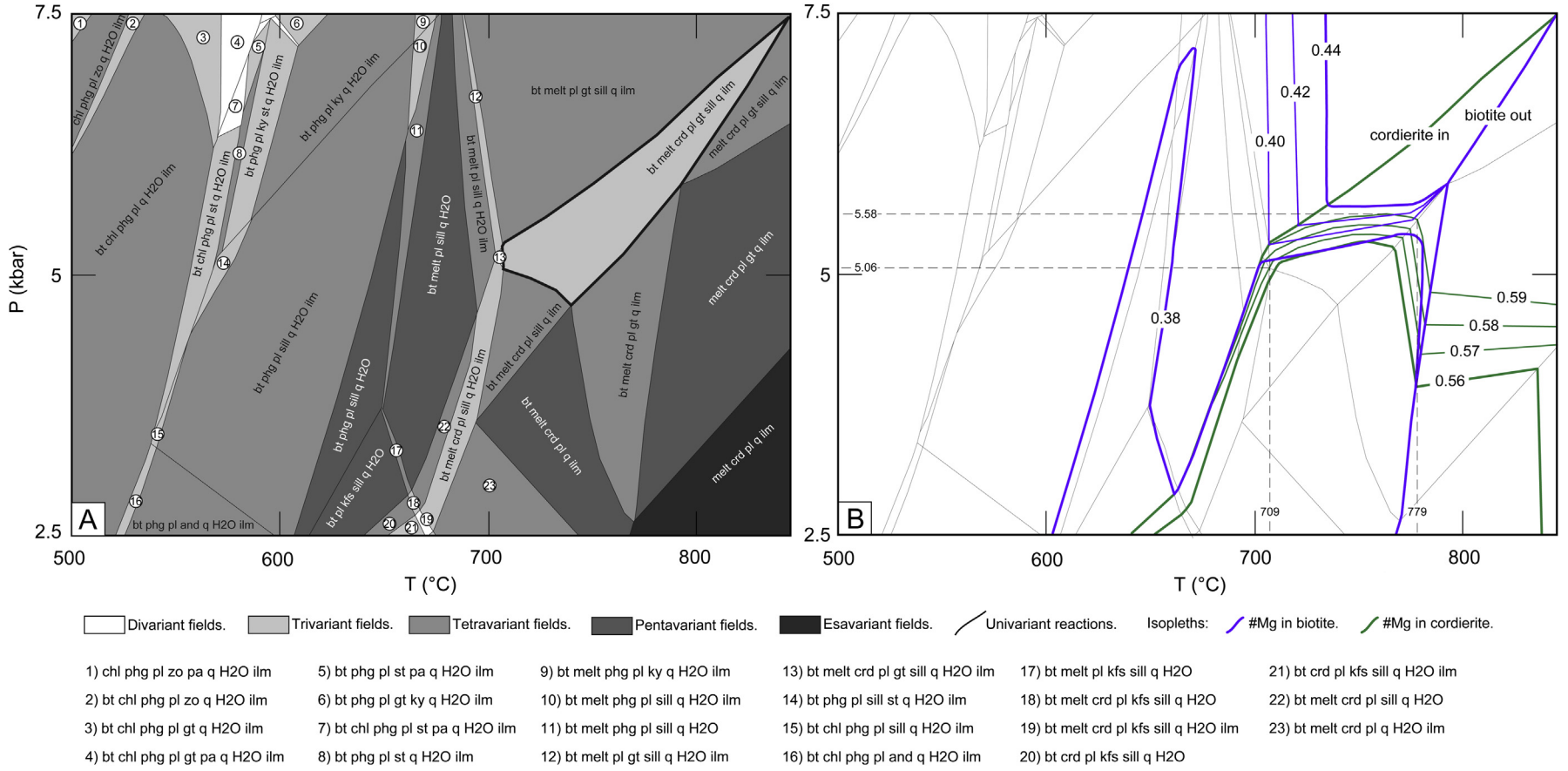

Fig. 7. A) P-T pseudosection for the migmatitic La Pampa Gneisses, sample JA05. Abbreviations for solid solutions and pure phases are: bt: biotite; gt: garnet; pl: plagioclase; kfs: potassium feldspar; ilm: ilmenite-geikielite-pyrophanite solution; crd: cordierite; phg: white mica; chl: chlorite; melt: hydrous silicated melt; zo: zoisite; pa: paragonite; q: quartz; st: staurolite; and: andalusite; ky: kyanite; sill: sillimanite; H2O: water. B) Isopleths of #Mg in cordierite and biotite projected over the stability fields of the pseudosection in Fig. 7a, showing the isopleth intersection stability field and the estimated minimum and maximum P and T for the peak conditions of metamorphism. The chemical composition of sample JA05 is presented in Table 1. The P-T pseudosection was calculated for the KNCFMASHT system, with normalized chemical composition (in wt % of major oxides): SiO_2: 69.64, TiO_2: 0.59, Al_2O_3: 14.73, FeO: 4.13, MgO: 1.42, CaO: 1.18; Na_2O: 1.72, K_2O: 2.68, H_2O: 3.92.

muscovite presents no deformation, whereas sillimanite, biotite and cordierite are deformed, furthermore it partially replaces biotite and cordierite (Fig. 4), so we conclude that muscovite grew during the retrograde path.

The intersection of isopleths (Fig. 7b) corresponding to the observed composition of biotite (#Mg = 0.38 to #Mg = 0.44) and cordierite (#Mg = 0.56 to #Mg = 0.59) occurs at 709–779 °C and 5.06–5.58 kbar within the field bt-melt-crd-pl-gt-sill-q-ilm (Fig. 7a). This field contains garnet, which is not observed in the sample. Although the predicted amount of garnet at the calculated conditions is low (around 1.6 wt%), this inconsistency is better explained in terms of accuracy of the calculations derived from the lack of consideration of Fe^{3+}, uncertainty in the amount of water present during partial melting, and the uncertainties inherent to standard thermodynamic properties of end members and solution models.

7. Discussion

The La Pampa Gneisses were originally considered as a candidate to be a remnant of the Chilenia basement in Chile (Ramos et al., 1986; Ribba et al., 1988). Nevertheless, as Chilenia w accreted to Gondwana during the Middle Devonian at *ca.* 390 Ma (Willner et al., 2011; Davis et al., 1999) and the age of the protolith of the La Pampa Gneisses is Pennsylvanian (306.5 ± 1.8 Ma) the suggestion that the La Pampa Gneisses could be part of Chilenia basement is clearly untenable. The genesis of the igneous protolith of the La Pampa Gneisses seems to have involved the partial melting of a sediment rich continental source in the Pennsylvanian at 306.5 ± 1.8 Ma, suggested by its high Al_2O_3 (15.02 wt%) content, the euhedral morphology of most of the zircon grains and the occurrence of centimetric recrystallized porphyroclasts of plagioclase. Magmatism at this time is recorded, in the El Tránsito valley area, by the zircon U–Pb ages of 300.8 ± 4.6 Ma reported by Salazar et al. (2009) for the acid volcanic and pyroclastic Cerro Bayo Formation and 296.1 ± 4.8 Ma for the Cerro Bayo Pluton (Coloma et al., 2012, Fig. 2). The age of the formation of the igneous protolith broadly coincides with the 320–300 Ma radiometric ages available for the older intrusive phases of the Elqui–Limarí Batholith (Nasi et al., 1985; Mpodozis and Kay, 1992; Hervé et al., 2013) which comprise large granitoid plutons showing an important crustal component in the magma source, i.e. high $^{87}Sr/^{86}Sr$ ratios (Mpodozis and Kay, 1992), high $\delta^{18}O$ and low εHf in zircons (Hervé et al., 2013). These intrusives include some peraluminous, muscovite-bearing intrusives such as those forming the Cochiguás Pluton in the Elqui valley region (Mpodozis and Cornejo, 1988).

Subsequently, during the Permian, the peraluminous Pennsylvanian intrusive rocks were metamorphosed under prograde conditions reaching peak metamorphism at a maximum of 779 °C and 5.58 kbar (Figs. 7 and 8) evidenced by the 267.6 ± 2.1 Ma zircon U–Pb age peak from sample JA05 (Fig. 5). This event was also recorded by Hervé et al. (2013), who analyzed by SHRIMP zircons from another sample of the La Pampa Gneisses (Sample FO10101) from which they obtained also a robust Carboniferous age peak (305,9.6 ± 2.7 Ma) but only two Permian ages around 270 Ma. This episode of metamorphism concurs with a regional Permian magmatic event during which the La Totora Pluton of 266.1 ± 3.5 Ma (Figs. 3 and 8) was emplaced. These ages seems to approximately coincide with the mid-Permian San Rafael Orogenic event that affected large parts of the Andean margin from northern Chile to the Frontal Cordillera in Argentina (see Llambías and Sato, 1990; Kleiman and Japas, 2009; Tomlinson et al., 2012). Mpodozis and Kay (1990, 1992) connect this event with the collision from the west of the hypothetical Terrane X, that may have shut-off Carboniferous-early Permian subduction along the Chilean segment of the Gondwana margin. During the Middle Triassic, 30 My after being metamorphosed, the gneisses were intruded by the La Pampa Pluton (241.7 ± 3 and 247 ± 3.1 Ma; Figs. 2 and 3). This magmatic activity would have responsible for the formation of the migmatitic contact metamorphism aureole surrounding the La Pampa Gneisses outcrops, and with recent data reported by Hervé et al. (2013), who obtained Triassic U–Pb SHRIMP ages with a peak of 238.9 ± 2.4 Ma in the external part of the metamorphic zircons from the La Pampa Gneisses (sample FO10101). The ages from the La Pampa Pluton are also concordant with the well constrained bulk rock, muscovite and biotite Rb/Sr isochron of 246 ± 18 Ma of the La Pampa Gneisses

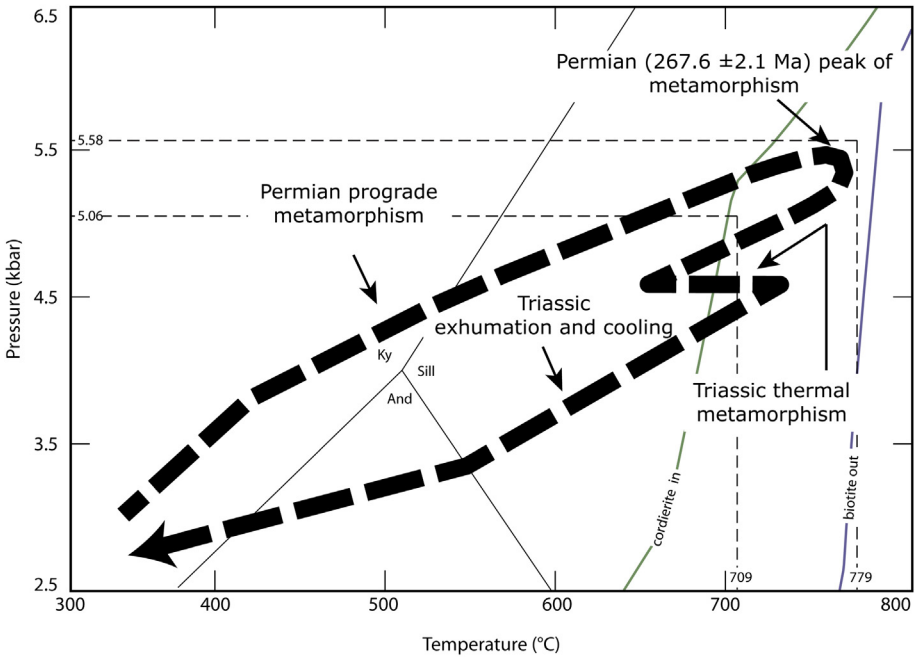

Fig. 8. A schematic clockwise P-T path for the metamorphic evolution of sample JA05 from the La Pampa Gneisses.

published by Ribba et al. (1988). The importance of this Middle Triassic magmatic event is reinforced by the new U–Pb zircon age we have acquired from the Conay Pluton (247.7 ± 3.4 Ma; Fig. 3), just to the east of the La Plata Fault (Fig. 2). The youngest radiometric ages available for the La Pampa Gneisses are two K/Ar of 239 ± 10 Ma in muscovite and 236 ± 6 Ma in biotite (Ribba et al., 1988), which are identical within errors to the K/Ar muscovite ages of 238 ± 10, 231 ± 6 and 229 ± 6 Ma also available for the El Tránsito Metamorphic Complex (Ribba et al., 1988) and, together, indicate a regional Triassic cooling event (Fig. 8). It is worth to mention that, at this time (Anisian–Ladinian) a thick sequence of more than 5 km of marine continental sediments (San Félix Formation; Zeil and Ichikawa, 1958; Reutter, 1974; Schoener, 1985; Padel et al., 2012) were accumulated in an extensional half graben to the west of the La Pampa region (Río del Carmen valley; Fig. 2). Cooling appears to be in response to extension-driven exhumation of the basement during a rifting episode that also affected, after the San Rafael event, large tracts of the Andean region during the Triassic (i.e. Mpodozis and Cornejo, 1997; Zerfass et al., 2004; Spalletti et al., 2008; Salazar et al., 2009). All these data can be integrated into a clockwise P-T-t path that shows the metamorphic evolution of the La Pampa Gneisses and includes regional prograde metamorphism during the Permian with a peak at 267.6 ± 2.1 Ma, thermal impact throughout the emplacement of the Triassic intrusives at *ca*. 240 Ma and retrograde exhumation and cooling as a consequence of extensional tectonics between 240 and 230 Ma (Fig. 8). A similar clockwise P-T-t path has been established by Soto et al. (2012) for the Permian to Triassic evolution of the Limón Verde Metamorphic Complex, which crops out further north, near Calama. Maximum pressures (7.5–14 Kbar) attained during the Permian metamorphic peak (which there seems to be older: 280 Ma) were, however, higher than those reached in the La Pampa Gneisses.

8. Conclusions

The La Pampa Gneisses are orthogneisses that form a large enclave in the Permian to Triassic Chollay Batholith, whose thermal and metamorphic evolution records a sequence of events that characterize the evolution of the Cordillera Frontal of north-central Chile between the late Carboniferous and Triassic. The protolith of the La Pampa Gneisses derives from peraluminous tonalites emplaced during the Pennsylvanian at 306.5 ± 1.8 Ma during a regional magmatic event, which included at least partial melting or involvement of a sedimentary source containing inherited zircons which crystallized during the Grenvillian, Pampean and Famatinian orogenies. The crystallization age of the La Pampa Gneisses protolith invalidates earlier proposals that considered this metamorphic unit as a possible remnant of the pre-collisional basement of the Chilenia terrane because this terrane was accreted to Gondwana during the middle Devonian (*ca*. 390 Ma). After being emplaced, the La Pampa Gneisses were metamorphosed under P-T conditions between 5.06 and 5.58 kbar and 709–779 °C during the middle Permian (*ca*. 267 Ma) concomitant with the oldest magmatic event recognized in the Chollay Batholith. A new intrusive episode linked to the emplacement of the La Pampa Pluton in the Middle Triassic (*ca*. 240 Ma) is recorded in the metamorphic rims of zircons and the Rb/Sr isotopic system while the slightly younger (*ca*. 239 Ma, muscovite; *ca*. 236 Ma, biotite) K/Ar ages can be, finally, interpreted as the result of very rapid exhumation and cooling during a Triassic regional episode of extension.

Acknowledgments

JA is grateful to Juan Vargas and Jaime Martínez (Universidad de Chile) for mineral separation and chemical analysis, respectively, Juan Cárdenas (Universidad de Granada) for substantial assistance provided during the use of the microprobe and Francisco Hervé, Jacobus Le-Roux and Fernando Sepúlveda for their help in reviewing this manuscript. This work was supported by Chilean Fondecyt Projects 1070964 and 1080468 and by Project CGL2009-12446 of the Ministry of Science and Innovation (MICINN), Spain. The results obtained in this manuscript are part of the doctoral thesis of JA, financed by a Conicyt (Chile) grant. Part of the results was obtained under a grant of the Departamento de Postgrado y Postítulo, Universidad de Chile. Authors thank to Claudio de Morisson Valeriano (Rio de Janeiro, Brazil) and Arne Willner (Bochum, Germany) for their helpful reviews comments.

Appendix A. Analytical methods

Zircon separation and geochronological analysis

Zircons were separated from three samples of plutonic rocks (JA01, JA02 and JA94) and one sample of the La Pampa Gneisses (JA05) using standard mineral separation techniques in the Department of Geology at the Universidad de Chile. After crushing and sieving at <500 mm, zircon grains were separated using a Gemini Table, a Frantz magnetic separator and heavy liquids (bromoform and methylene iodide). Final zircon selection was made by hand-picking under a binocular microscope. Zircon grains from each sample were mounted in a 1-inch diameter epoxy puck that was ground and polished to expose the grains. Photomicrograph maps and cathodoluminescence images were used to characterize the internal features of zircons such as growth zones and inclusions and to provide a base map for recording laser spot locations. Approximately 50 zircon grains were analyzed for each sample. U–Pb analyses were conducted by laser ablation inductively coupled plasma mass spectrometry (LA-ICP-MS) at the Radiogenic Isotope and Geochronology Laboratory at Washington State University, using a New Wave Nd:YAG UV-213 nm laser ablation system coupled to a ThermoFinnigan Element2 single collector double-focusing magnetic sector ICP-MS, following the analytical procedures described in Chang et al. (2006). The collector configuration allows measurement of ^{204}Pb in an ion-counting channel while ^{206}Pb, ^{207}Pb, ^{208}Pb, ^{232}Th and ^{238}U are simultaneously measured with Faraday detectors. However, common Pb is typically not significant in LA-ICP-MS analyses, most likely because it is concentrated in cracks and inclusions, which can be avoided (Gaschnig et al., 2009). All analyses were conducted in static mode with a laser beam diameter of 35 μm, operated with output energy of ~32 mJ (at 23 kV) and a pulse rate of 10 Hz. Each analysis consisted of one 12-s integration on peaks with no laser firing and 21-s integrations on peaks with laser firing. Hg contribution to the ^{204}Pb mass position was removed by subtracting on-peak background values. The lead isotopic ratios were corrected for common Pb, using the measured ^{204}Pb, assuming an initial Pb composition according to Stacey and Kramers (1975) and respective uncertainties of 1.0, 0.3 and 2.0 for ^{206}Pb/^{204}Pb, ^{207}Pb/^{204}Pb, and ^{208}Pb/^{204}Pb. For this study we used two zircon standards: Peixe (Dickinson and Gehrels, 2003) and FC-1 (Paces and Miller, 1993). U–Pb ages were calculated using Isoplot (Ludwig, 2003). Ages with >25% discordance or >5% reverse discordance are considered unreliable and were not used. Also, analyses with an error greater than 10% were rejected.

Whole rock and mineral analysis

Analysis of sample JA05 was obtained by J. Martinez with a Perkin Elmer Inductively Coupled Plasma Optical Emission Spectrometer (ICP-OES) OPTIMA 7400V model, at the Department of

Geology, Universidad de Chile. The standard used was BHVO2 from USGS, Table A1 shows the details (RV: recommended value, MV: measurement value from average of 4 analyzes).

Table A1

BHVO 2	RV	MV	SD
SiO_2%	49.9	49.7	±0.35
Al_2O_3	13.5	13.4	±0.11
TiO_2	2.73	2.68	±0.02
CaO	11.4	11.2	±0.10
Fe_2O_3	12.3	12.0	±0.12
MgO	7.23	7.27	±0.10
MnO	0.17	0.18	±0.015
Na_2O	2.22	2.24	±0.12
K_2O	0.52	0.54	±0.03
P_2O_5	0.27	0.26	±0.010

Minerals of sample JA05 were analysed using a CAMECA SX100 electron microprobe at the Universidad de Granada, Spain. The instrumental conditions used were a 15 kV accelerating voltage, 15 nA beam current and 5 mm beam diameter. Standards used for element calibrations were natural minerals: sanidine (K), barite (Ba), vanadinite (Cl), diopside (Ca), rutile (Ti), albite (Na), quartz (Si), and synthetic oxides: Fe_2O_3 (Fe), $MnTiO_3$ (Mn), Cr_2O_3 (Cr), MgO (Mg) and Al_2O_3 (Al).

References

Álvarez, J., Mpodozis, C., Arriagada, C., Astini, R., Morata, D., Salazar, E., Valencia, V., Vervoort, J., 2011. Detrital zircons from late Paleozoic accretionary complexes in north-central Chile (28°–32°S): possible fingerprints of the Chilenia terrane. Journal of South American Earth Sciences 32, 460–476.

Astini, R., Benedetto, J., Vaccari, N., 1995. The early Paleozoic evolution of the Argentine Precordillera as a Laurentian rifted, drifted, and collided terrane: a geodynamic model. Geological Society of America Bulletin 107, 253–273.

Astini, R., Dávila, F., 2004. Ordovician back arc foreland and Ocloyic thrust belt development on the western Gondwana margin as a response to Precordillera terrane accretion. Tectonics 23 (TC4008), 19. http://dx.doi.org/10.1029/2003TC001620.

Astini, R., Cawood, P., 2009. A Proterozoic basement under the northern Cordillera Frontal: a hint to Chilenia and the continuation of the accretionary prism east of Precordillera?. In: XII Congreso Geológico Chileno, Abstract S9_01 2, Santiago.

Cawood, P., 2005. Terra Australis Orogen: Rodinia breakup and development of the Pacific and Iapetus margins of Gondwana during the Neoproterozoic and Paleozoic. Earth-Science Reviews 69, 249–279.

Chang, Z., Vervoort, J., McClelland, W., Knaack, C., 2006. U-Pb dating of zircon by LA-ICP-MS. Geochemistry, Geophysics, Geosystems 7, Q05009.

Chew, D., Magnab, T., Kirkland, C., Miskovic, C., Cardona, A., Spikings, R., Schaltegger, U., 2008. Detrital zircon fingerprint of the Proto-Andes: evidence for a neoproterozoic active margin? Precambrian Research 167, 186–200.

Coira, B.L., Kay, S.M., Pérez, B., Woll, B., Hanning, M., Flores, P., 1999. Magmatic sources and tectonic setting of Gondwana margin Ordovician magmas, northern Puna of Argentina and Chile. In: Ramos, V.A., Keppie, D. (Eds.), Laurentia Gondwana Connections before Pangea, Geological Society of America Special Paper 336, pp. 145–170.

Coloma, F., Salazar, E., Creixell, C., 2012. Nuevos antecedentes acerca de la construcción de los plutones Pérmicos y Permo-Triásicos en el valle del río Tránsito, región de Atacama, Chile. In: XIII. Congreso Geológico Chileno Abstract S3_023, Antofagasta.

Connolly, J., 2005. Computation of phase equilibria by linear programming: a tool for geodynamic modeling and its application to subduction zone decarbonation. Earth and Planetary Science Letters 236, 524–541.

Cordani, U.G., Fraga, L.M., Reis, N., Tassinari, C., Brito-Neves, B., 2010. On the origin and tectonic significance of the intra-plate events of Grenvillian-type age in South America: a discussion. Journal of South American Earth Sciences 29, 143–159.

Davis, J., Roeske, S., McClelland, W., Kay, S., 2000. Mafic and ultramafic crustal fragments of the southwestern Precordillera terrane and their bearing on tectonic models of the early Paleozoic in western Argentina. Geology 28, 171–174.

Davis, J., Roeske, S., McClelland, W., Snee, L., 1999. Closing the ocean between the Precordillera terrane and Chilenia: early Devonian ophiolite emplacement and deformation in the southwest Precordillera. In: Ramos, V.A., Keppie, J.D. (Eds.), Laurentia-Gondwanan connections before Pangea, Geological Society of America Special Paper 336, p. 115e138.

Dickinson, W.R., Gehrels, G.E., 2003. U-Pb ages of detrital zircons from Permian and Jurassic eolianite sandstones of the Colorado Plateau, USA: paleogeographic implications. Sedimentary Geology 163, 29–66.

Gaschnig, R., Vervoort, J., Lewis, R., McClelland, W., 2009. Migrating magmatism in the northern US Cordillera: in situ U–Pb geochronology of the Idaho batholith. Contributions to Mineralogy and Petrology 159, 863–883. http://dx.doi.org/10.1007/s00410-009-0459-5.

Godoy, E., Wellkner, D., 2003. El Basamento de la Costa del Norte Chico, 20 años después. In: X Congreso Geológico Chileno. CD ROM, Concepción.

González-Menéndez, L., Gallastegui, G., Cuesta, A., Heredia, N., Rubio-Ordóñez, A., 2013. Petrogenesis of Early Paleozoic basalts and gabbros in the western Cuyania terrane: constraints on the tectonic setting of the southwestern Gondwana margin (Sierra del Tigre, Andean Argentine Precordillera). Gondwana Research 24, 359–376.

Hervé, F., 1988. Late Paleozoic subduction and accretion in Southen Chile. Episodes 11, 183–188.

Hervé, F., Calderón, M., Fanning, C.M., Pankhurst, R.J., Godoy, E., 2012. Provenance variations in the Late Paleozoic accretionary complex of central Chile as indicated by detrital zircons. Gondwana Research. http://dx.doi.org/10.1016/j.gr.2012.06.016.

Hervé, F., Fanning, M., Calderón, M., Mpodozis, C., 2013. Early Permian to Late Triassic batholiths of the Chilean Frontal Cordillera (28°–31°S): SHRIMP U–Pb zircon ages and Lu–Hf and O isotope systematic. Lithos (submitted for publication).

Holland, T., Powell, R., 1998. An internally consistent thermodynamic data set for phases of petrological interest. Journal of Metamorphic Geology 16 (3), 309–343.

Hoskin, P., Schaltegger, U., 2003. The composition of zircon and igneous and metamorphic petrogenesis. Reviews in Mineralogy and Geochemistry 53, 27–62.

Irwin, J., García, C., Hervé, F., Brook, M., 1988. Geology of part of a long-lived dynamic plate margin: the coastal cordillera of north-central Chile, latitude 30°51′–31°S. Canadian Journal of Earth Sciences 25, 603–624.

Kay, S., Ramos, V., Mpodozis, C., Sruoga, P., 1989. Late Paleozoic to Jurassic silicic magmatism at the Gondwana margin: analogy to the Middle Proterozoic in North America? Geology 17, 324–328.

Keppie, J., Ramos, V., 1999. Odyssey of Terranes in the Iapetus and Rheic Oceans during the Paleozoic. Geological Society of America, pp. 267–276. Special Paper 336.

Kleiman, L.E., Japas, M.S., 2009. The Choiyoi volcanic province at 34 S–36 S (San Rafael, Mendoza, Argentina): Implications for the late Palaeozoic evolution of the southwestern margin of Gondwana. Tectonophysics 473 (3), 283–299.

Lee, J., Williams, I., Ellis, D., 1997. Pb, U, and Th diffusion in natural zircon. Nature 390, 159–162.

Llambías, E.J., 1999. Las rocas ígneas Gondwánicas: El magmatismo Gondwánico durante el Paleozoico superior-Triásico. In: Caminos, R. (Ed.), Geología Argentina. Servicio Geológico Minero Argentino, Buenos Aires, pp. 349–363.

Llambías, E.J., Sato, A.M., 1990. El Batolito de Colanguil (29–31° S): estructuras y marco tectónico, Cordillera Frontal de Argentina. Revista Geológica de Chile 17 (1), 89–108.

López de Azarevich, V., Escayola, M., Azarevich, M., Pimentel, M., Tassinari, C., 2009. The Guarguaraz Complex and the Neoproterozoic-Cambrian evolution of southwestern Gondwana: geochemical signatures and geochronological constraints. Journal of South American Earth Sciences 28, 333–344.

Ludwig, K.R., 2003. Isoplot 3.0. A Geochronological Toolkit for Microsoft Excel. Special publication No. 4. Berkeley Geochronology Center, Berkeley, Calif, p. 71.

Martin, M., Clavero, J., Mpodozis, C., 1999. Late Paleozoic to early Jurassic tectonic development of the high Andean Principal Cordillera, El Indio Region, Chile (29–30° S). Journal of South American Earth Sciences 12, 33–49.

Massonne, H., Calderón, M., 2008. P-T evolution of metapelites from the Guarguaraz Complex, Argentina: evidence for Devonian crustal thickening close to the western Gondwana margin. Revista Geológica de Chile 35 (2), 215–231.

Moscoso, R., Nasi, C., Salinas, P., 1982. Hoja Vallenar y Parte Norte de La Serena, Regiones de Atacama y Coquimbo. In: Carta Geológica de Chile, vol. 55. Servicio Nacional de Geología y Minería, Santiago.

Mpodozis, C., Cornejo, P., 1988. Hoja Pisco Elqui, Región de Coquimbo. In: Carta Geológica de Chile. Servicio Nacional de Geología y Minería, p. 164. No. 68 (1: 250.000).

Mpodozis, C., Cornejo, P., 1997. El Rift Triásico-Sinemuriano de Sierra Exploradora, Cordillera de Domeyko (25°26′ S) Asociaciones de facies y Reconstrucción Tectónica. In: VIII Congreso Geológico Chileno. Actas, vol. 1. Antofagasta, pp. 550–554.

Mpodozis, C., Kay, S.M., 1990. Provincias magmáticas ácidas y evolución tectónica de Gondwana: Andes chilenos (28–31° S). Revista Geológica de Chile 17 (2), 153–180.

Mpodozis, C., Kay, S., 1992. Late Paleozoic to Triassic evolution of the Gondwana margin: evidence from Chilean Frontal Cordilleran batholiths (28°S to 31°S). Geological Society of America Bulletin 104, 999–1014.

Murillo, I., 2012. Geología estructural del valle de El Tránsito, con énfasis en las Milonitas El Portillo y su relación con la evolución tectónica desde el Paleozoico superior en Chile, entre los 28°40′–29°04′ S. Thesis (Unpublished). Departamento de Geología, Universidad de Chile, Santiago.

Nasi, C., Mpodozis, C., Cornejo, P., Moscoso, R., Maksaev, V., 1985. El Batolito Elqui-Limarí (Paleozoico Superior-Triásico): características petrográficas, geoquímicas y significado tectónico. Revista Geológica de Chile 25–26, 77–111.

Paces, J., Miller, J., 1993. Precise U–Pb ages of Duluth complex and related mafic intrusions, northeastern Minnesota; geochronological insights to physical, petrogenetic, paleomagnetic, and tectonomagmatic processes associated with the 1.1 Ga midcontinent rift system. Journal of Geophysical Research 98 (B8). http://dx.doi.org/10.1029/93JB01159.

Padel, M., Salazar, E., Coloma, F., 2012. Arquitectura y evolución tectonoestratigráfica del Depocentro de San Félix, Triásico medio a superior: Resultados preliminares. In: XIII. Congreso Geológico Chileno Abstract S5_004, Antofagasta.
Pankhurst, R., Millar, I., Hervé, F., 1996. A Permo-Carboniferous U-Pb age for part of the Guanta Unit of the Elqui-Limari Batholith at Río del Tránsito, Northern Chile. Revista Geológica de Chile 23 (1), 35–42.
Ramos, V., 2009. Anatomy and global context of the Andes: main geologic features and the Andean orogenic cycle. In: Kay, S.M., Ramos, V.A., Dickinson, W. (Eds.), Backbone of the Americas, Shallow Subduction, Plateau Uplift and Terrane Collision. Geological Society of America, pp. 31–66. Memoir 204.
Ramos, V., 2010. The Grenville-age basement of the Andes. Journal of South American Earth Sciences 29, 77–91.
Ramos, V., Basei, M., 1997. The basement of Chilenia: an exotic continental terrane to Gondwana during the early Paleozoic. In: Terrane Dynamics 97, International Conference on Terrane Geology, pp. 140–143. Christchurch, New Zealand, Conference Abstracts.
Ramos, V., Jordan, T., Allmendinger, R., Kay, S., Cortés, J., Palma, M., 1984. Chilenia: Un terreno alóctono en la evolución paleozoica de los Andes Centrales. In: IX Congreso Geológico Argentino, vol. 2, pp. 84–106.
Ramos, V., Jordan, T., Allmendinger, R., Mpodozis, C., Kay, S., Cortés, J., Palma, M., 1986. Paleozoic terranes of the central Argentine-Chilean Andes. Tectonics 5, 855–880.
Rapela, C., Pankhurst, R., Casquet, C., Baldo, E., Saavedra, J., Galindo, C., Fanning, C., 1998. The Pampean Orogeny of the southern proto-Andes: Cambrian continental collision in the Sierras de Córdoba. In: Geological Society, London, Special Publications 142, pp. 181–217.
Reutter, K., 1974. Entwicklung und Bauplan der chilenischen Hochkordillere im Bereich 29° südlicher Breite. Neues Jahrbuch für Geologie und Paläontologie 146 (2), 153–178.
Ribba, L., 1985. Geología regional del cuadrángulo El Tránsito, región de Atacama, Chile. Thesis (Unpublished). Departamento de Geología, Universidad de Chile, Santiago.
Ribba, L., Mpodozis, C., Hervé, F., Nasi, C., Moscoso, R., 1988. El basamento del Valle del Tránsito, Cordillera de Vallenar: eventos magmáticos y metamórficos y su relación con la evolución de los andes chileno-argentinos. Revista Geológica de Chile 15, 126–149.
Salazar, E., Arriagada, C., Mpodozis, C., Martínez, F., Peña, M., Álvarez, J., 2009. Análisis Estructural del Oroclino de Vallenar: Primeros Resultados. In: XII Congreso Geológico Chileno Abstract S9_026, Santiago.
Salazar, E., Mpodozis, C., Arriagada, C., Coloma, F., 2012. Evolución tectonoestratigráfica post-paleozoica de la Cordillera de Vallenar. In: XIII. Congreso Geológico Chileno Abstract S2_027, Antofagasta.
Schoener, F., 1985. Stratigraphisch-Iazielle Entwicklung der Trias im Gebiet von Vallenar, Region de Atacama (Chile). Berliner Geowissenschaft, Serie A 2, 99.
Schwartz, J., Gromet, P., Miró, R., 2008. Timing and duration of the Calc-Alkaline arc of the Pampean Orogeny: implications for the Late Neoproterozoic to Cambrian evolution of Western Gondwana. The Journal of Geology 116, 39–61.
Soto, M.F., Hervé, F., Calderón, M., Massone, M., Fanning, C.M., 2012. Pressure-temperature time paths for the Limón Verde Metamorpic Complex, Chile. In: XIII Congreso Geológico Chile. Actas, vols. 362–364. Antofagasta.
Spalletti, L.A., Fanning, C.M., Rapela, C.W., 2008. Dating the Triassic continental rift in the southern Andes: the Potrerillos Formation, Cuyo Basin, Argentina. Geologica Acta: An International Earth Science Journal 6, 267–283.
Stacey, J., Kramers, J., 1975. Approximation of terrestrial lead isotope evolution by a two-stage model. Earth and Planetary Science Letters 26, 207–221.
Thomas, W., Astini, R., 2003a. The Argentine Precordillera: a traveler from the Ouachita embayment of north American Laurentia. Science 273 (5276), 752–757.
Thomas, W., Astini, R., 2003b. Ordovician accretion of the Argentine Precordillera terrane to Gondwana: a review. Journal of South American Earth Sciences 16, 67–79.
Tomlinson, A., Blanco, N., García, M., Baez, L., Alcota, H., Ladino, M., Pérez de Arce, C., Fanning, C.M., Martin, M., 2012. Permian exhumation of metamorphic complexes in the Calama area: evidence for flat-slab subduction in northern Chile during the San Rafael tectonic phase and origin of the Central Andean Gravity High. In: XIII Congreso Geológico de Chile, Actas, 209.211, Antofagasta.
Torres-Roldán, R., García-Casco, A., García-Sanchez, P., 2000. CSpace: an integrated workplace for the graphical and algebraic analysis of phase assemblages on 32-bit wintel platforms. Computers and Geosciences 26, 779–793.
Welkner, D., Arévalo, C., Godoy, E., 2006. Geología del Area Freirina-El Morado. In: Carta geológica de Chile, Serie Geología Básica, vol. 100. Servicio Nacional de Geología y Minería, Santiago.
Willner, A.P., Gerdes, A., Massonne, H.J., 2008. History of crustal growth and recycling at the Pacific convergent margin of South America at latitudes 29°–36° S revealed by a U–Pb and Lu–Hf isotope study of detrital zircon from late Paleozoic accretionary systems. Chemical Geology 253, 114–129.
Willner, A.P., Gerdes, A., Massonne, H.J., Schmidt, A., Sudo, M., Thomson, S.N., Vujovich, G., 2011. The geodynamics of collision of a microplate (Chilenia) in Devonian times deduced by the pressure-temperature-time evolution within part of a collisional belt (Guarguaraz Complex, W-Argentina). Contributions to Mineralogy and Petrology 162, 303–327. http://dx.doi.org/10.1007/s00410-010-0598-8.
Zeil, W., Ichikawa, K., 1958. Marine Mitllere-Trias in der Hochkordillere der Provinz Atacama (Chile). Neues Jahrbuch für Peologie und Palantologie 106, 339–351.
Zerfass, H., Chemale, F., Schultz, C., Lavina, E., 2004. Tectonics and sedimentation in Southern South America during Triassic. Sedimentary Geology 166, 265–292.